AD-A094 456 CALIFORNIA UNIV BERKELEY ELECTRONICS RESEARCH LAB F/G 20/9
PLASMA THEORY AND SIMULATION.(U)
MAR 80 C K BIRDSALL N00014-77-C-0578

UNCLASSIFIED

END
DATE FILMED
2-81
DTIC

(9) FIRST QUARTER PROGRESS REPORT. no. 1, 1 Jan-31 Mar 80,

(6) PLASMA THEORY and SIMULATION.

January 1 to March 31, 1980

(12) 75

Research during the First Quarter of 1980 is reported here.

Our research group uses both theory and simulation as tools in order to increase the understanding of instabilities, heating, transport, and other phenomena in plasmas. We also work on the improvement of simulation, both theoretically and practically.

Our staff is (10)

Professor C. K. Birdsall *Principal Investigator*	191 M	Cory Hall	(642-4015)
Alex Friedman *Post Doctorate*	119 ME	Cory Hall	(642-3477)
Bruce Cohen, William Nevins *Lecturers UCB; Physicists LLL*	L439 L439	LLL LLL	(422-9823) (422-7032)
William Fawley *Guest UCB; Physicist LLL*	L321	LLL	(422-9272)
Yu Jiuan Chen, Douglas Harned, Vincent Thomas, Niels Otani, Jin Soo Kim *Research Assistants*	119 MD	Cory Hall	(642-1297)
Stephen Au-Yeung *Programmer*	119 MD	Cory Hall	(642-1297)
Mike Hoagland *Research Typist*	199 M	Cory Hall	(642-7919)

(11) 31 Mar[illegible]80

DOE Contract AS03-76SF00034-DE-AT03-76ET53064
ONR Contract N00014-77-C-0578
(15) DE-AS03-76-SF-00034

ELECTRONICS RESEARCH LABORATORY

College of Engineering
University of California, Berkeley
94720

TABLE OF CONTENTS

*Indicates ONR supported areas.

Accession For	
NTIS GRA&I	X
DTIC TAB	☐
Unannounced	☐
Justification	
By	
Distribution/	
Availability Codes	
Dist	Avail and/or Special
A	

Section I

PLASMA THEORY AND SIMULATION

A. Lower Hybrid Drift Instability Simulations Using ES1 Hybrid Code

Yu-Jiuan Chen (Prof. C. K. Birdsall, B. I. Cohen)

The saturated electric field energy spectrum $\mathcal{E}_k$ due to ion trapping was obtained in theory and compared with simulation. These and all of the simulations will be given in an ERL report now in preparation, to be submitted to the Physics of Fluids.

B. Beaming Instabilities; Magnetized Rings

Jin Soo Kim (Prof. C. K. Birdsall, B. I. Cohen)

Our multi-ring instability study (the distribution of plasma in velocity space perpendicular to the magnetic field is a set of discrete rings) was begun with one, two and four rings. The one ring model produces the well known Dory-Guest-Harris instability.[1] The multi-ring model corresponds to multi-velocity neutral injection, as well as to initial conditions common to simulation models. The model has only ion rings because the electron Larmor radius (in terms of $k_\perp a_e$) is negligible compared with that of ions (in terms of $k_\perp a_i \sim 1$). In our current work, the rings in velocity space have equal weight (same ω_p^2) and are spaced at equal intervals, as shown in Fig. 1; the plasma is uniform in x space, as is the magnetic field.

The distribution function for N rings is the sum of δ-functions;

$$f_o(v_\perp, v_\parallel) = \frac{1}{N} \sum_{s=1}^{N} \frac{1}{2\pi v_{\perp s}} \delta(v_\perp - v_{\perp s})\, \delta(v_\parallel) \,. \qquad (1)$$

The dispersion relation of a single ring for perpendicular propagation ($k_\parallel = 0$) is

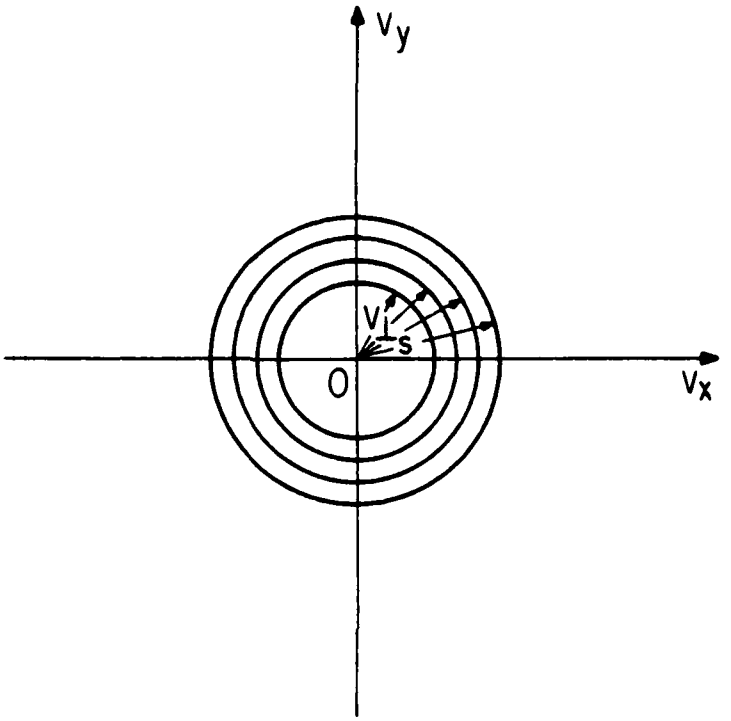

FIG. 1 Distribution of ions in $v_\perp$ space. The ring speeds are: for 2 rings, $v_{\perp 1} = 1-\alpha$, $v_{\perp 2} = 1+\alpha$; for 4 rings, $v_{\perp 1} = 1-3\alpha$, $v_{\perp 2} = 1-\alpha$, $v_{\perp 3} = 1+\alpha$, $v_{\perp 4} = 1+3\alpha$. The α values used so far are 0.00 to 0.06.

$$D(\omega,k_\perp) = 1 - \frac{\omega_p^2}{\omega_c^2} \sum_{n=-\infty}^{\infty} \frac{1}{\mu_\perp} \frac{dJ_n^2(\mu_\perp)}{d\mu_\perp} \frac{n\omega_c}{\omega - n\omega_c} \qquad (2)$$

where $\mu_\perp = k_\perp v_\perp/\omega_c$ and J_n is the Bessel function of the first kind of order n; this is Eq. (19) of Tataronis and Crawford[2]. Hence, for the multi-ring model of equal density rings the dispersion relation is (ignoring electrons)

$$D(\omega,k_\perp) = 1 - \frac{1}{N}\frac{\omega_p^2}{\omega_c^2} \sum_{s=1}^{N} \sum_{n=-\infty}^{\infty} \frac{1}{\mu_{\perp s}} \frac{dJ_n^2(\mu_{\perp s})}{d\mu_{\perp s}} \frac{n\omega_c}{\omega - n\omega_c} \quad . \qquad (3)$$

The roots of $D(\omega,k_\perp) = 0$ are obtained numerically, using the code, ROOTS[3,4].

Figures 2 and 3 shows the maximum growth rate for two rings; Figs. 4 and 5, for four rings. When ω_p^2/ω_c^2 is larger than the threshold values, some of the Bernstein modes couple to each other and the waves grow ($\gamma \equiv \text{Imag}(\omega) \neq 0$) as is well known. γ_{max} is the maximum value of γ of all Bernstein modes. The growth rates become smaller as number of rings goes from 1 to 2 and to 4 by spreading the distribution over $v_\perp$-space, corresponding to warming up the cold ring, a result found earlier[1]. As is shown in Fig. 3 and Fig. 5 the instability threshold values of ω_p^2/ω_c^2 become larger as the number of rings increases from 1 to 2 to 4.

These studies will be extended to larger values of the parameters and then to non-uniform envelopes of the rings, such as Maxwellian.

REFERENCES

1. R. A. Dory, G. E. Guest, and E. G. Harris, "Unstable Electrostatic Plasma Waves Propagating Perpendicular to a Magnetic Field", Phys. Rev. Lett. 5, 131 (1965).
2. J. A. Tataronis and F. W. Crawford, "Cyclotron Harmonic Wave Propagation and Instabilities; 1. Perpendicular Propagation", J. Plasma Phys. 4, 231 (1970).

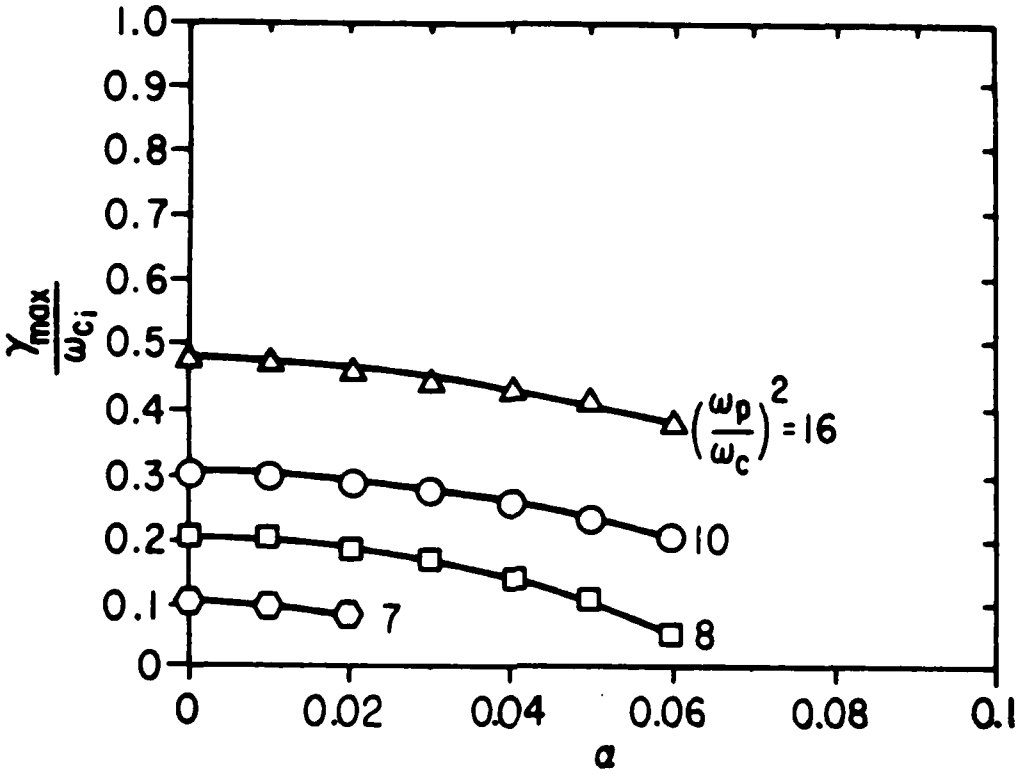

FIG. 2 Maximum growth rate vs. α (interval of rings) for 2 rings.

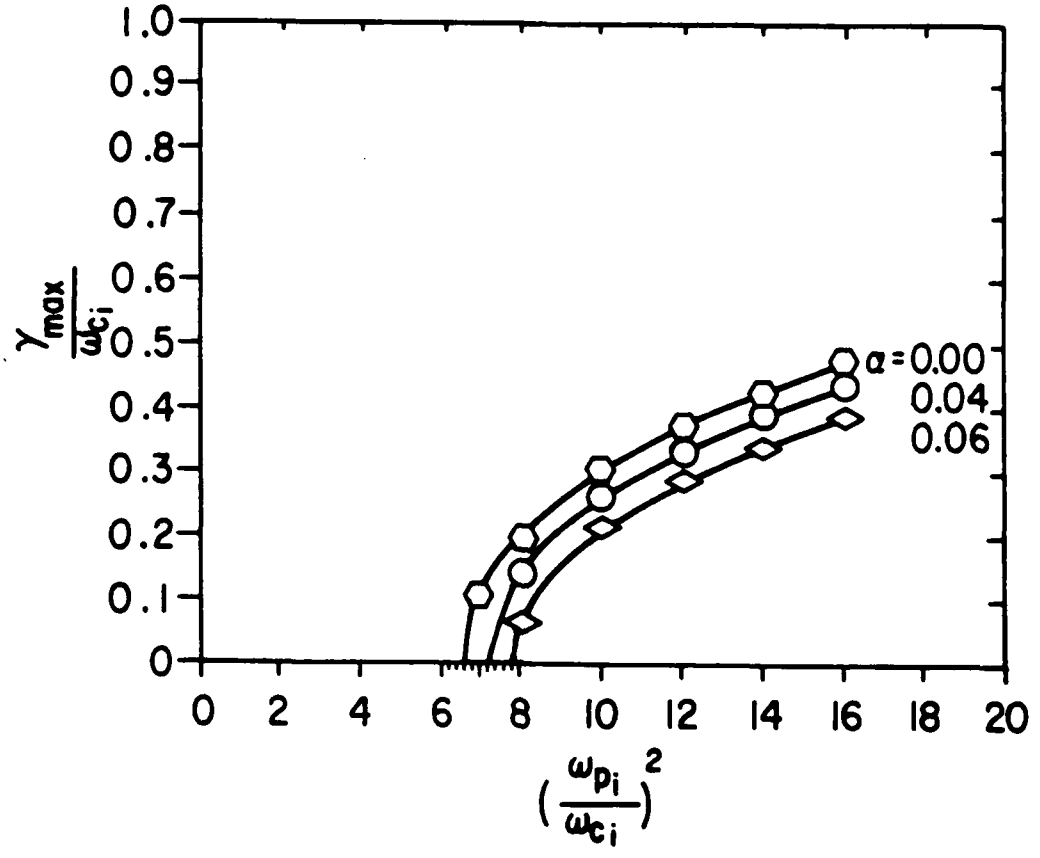

FIG. 3 Maximum growth rate vs. $(\omega_p/\omega_c)_i^2$ for two rings. The marginal stability values of $(\omega_p/\omega_c)_i^2$ are: 6.6 for a single ring ($\alpha = 0$) as also found in Table 1 of Tataronis and Crawford[1]; 7.2 (for $\alpha = 0.04$); 7.8 (for $\alpha = 0.06$).

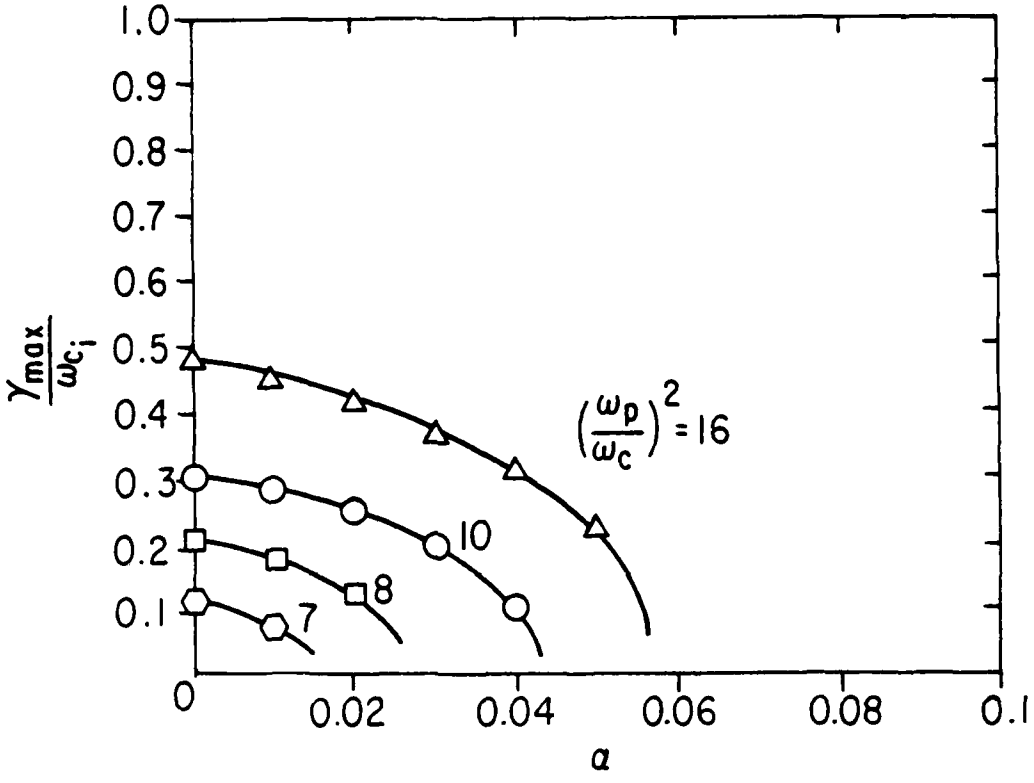

FIG. 4 Maximum growth rate vs. α (interval of rings) for 4 rings.

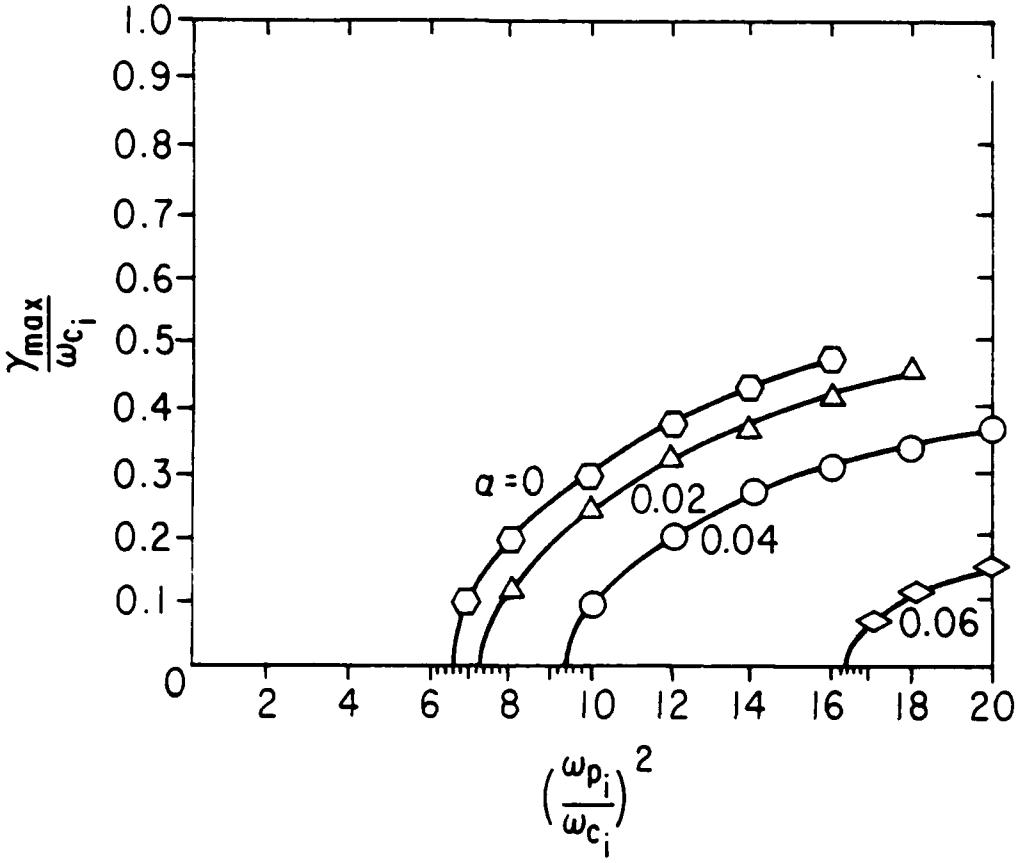

FIG. 5 Same as Fig. 3, for 4 rings. The marginal stability values of $(\omega_p/\omega_c)_i^2$ are 9.4 ($\alpha = 0.04$) and 16.3 ($\alpha = 0.06$).

3. M. J. Gerver, "ROOTS, A Dispersion Equation Solver", University of California, Berkeley, ERL Memorandum No. M77/27 (1976).

4. M. J. Gerver, C. K. Birdsall, A. B. Langdon and D. Fuss, "Normal Modes of a Loss Cone Plasma Slab with Steep Density Gradient", Phy. Fl. 20, pp. 291-300, Feb. 1977.

C. Field-Reversed Plasma Simulations, Quasineutral, in 2d

Douglas Harned (A. Friedman, C. K. Birdsall)

A realistic simulation of field-reversed layer stability problems requires a bounded system, normally bounded by conducting walls. Additionally, for a fusion reactor, the region near the walls should be a vacuum or cold gas. The replacement of the vacuum or cold gas region with a low density plasma is inadequate in a quasineutral model. When such a replacement is made, large electric field fluctuations occur, and a highly restrictive Courant condition ($\Delta t < \Delta x/v_A$, where v_A is the Alfven speed) is imposed in the low density regions. Our one dimensional simulations have shown that large amplitude waves occuring in the low density regions can distort the physics in the dense part of the plasma. It is not surprising to find such problems, since the quasineutrality assumption becomes invalid for low density. These difficulties seem to be inherent in explicit schemes for advancing the field quantities. A method which avoids such problems in low density regions has been developed by Hewett.[1] Hewett's method implicitly advances the fields and treats the vacuum, or near vacuum, by setting the resistivity to a large value.

Boundary conditions impose a further difficulty. This is because a quasineutral code does not model the details of the sheath region at the wall. This defect prevents the specification of reflecting wall boundaries in conjunction with conducting wall boundaries. At a conducting wall we know that

$$\hat{n} \times \underline{E} = 0 . \tag{1}$$

While this condition is insufficient to solve the field equations, the boundary condition

$$\hat{n} \cdot \underline{B} = 0 \tag{2}$$

implies that the longitudinal (curl-free) and transverse (divergence-free) parts of the tangential electric field (E_ℓ and E_t) must each vanish at the conductor. In terms of the potentials $\underline{A}$ and ϕ, in the Coulomb gauge, we have at the walls

$$\hat{n} \times \underline{A} = 0 \tag{3a}$$

$$\phi = \text{constant} \tag{3b}$$

where $\underline{A}$ and ϕ are such that $\underline{B} = \nabla \times \underline{A}$ and $E_\ell = -\nabla\phi$. With the gauge condition, $\nabla \cdot \underline{A} = 0$, the boundary conditions are sufficient to determine the advance of the field equations. It should be noted that in one-dimensional codes (such as our QUAD1) the boundary problem is trivial as the longitudinal and transverse parts of the electric field are geometrically decoupled.

The need for a bounded system and proper treatment of low density regions have motivated us to change the field solver in our two-dimensional, doubly periodic code. The following is a description of a method which may handle both problems.

The quasineutral field equations are

$$\underline{E} = \frac{1}{4\pi ne} (\nabla \times \underline{B}) \times \underline{B} - \frac{1}{nec} \underline{J} \times \underline{B} + \frac{cn}{4\pi} \nabla \times \underline{B} \tag{4}$$

$$\frac{\partial \underline{B}}{\partial t} = -c \nabla \times \underline{E}$$

where η is the resistivity, $\underline{J}$ the ion current density, and the electrons have been assumed to be cold. In terms of the vector potential $\underline{A}$, we have

$$\underline{E} = \frac{-1}{4\pi ne} \nabla^2 \underline{A} \times (\nabla \times \underline{A} + \underline{B}_o) - \frac{1}{nec} \underline{J} \times [(\nabla \times \underline{A}) \times \underline{B}_o] - \frac{c\eta}{4\pi} \nabla^2 \underline{A} \qquad (6)$$

$$\frac{\partial \underline{A}}{\partial t} = -c\underline{E}_t \qquad (7)$$

where $\underline{B} = \nabla \times \underline{A} + \underline{B}_o$. $\underline{B}_o$ represents a constant background magnetic field. Equations (6 and 7) can be combined to give

$$\frac{\partial \underline{A}}{\partial t} = \left\{ \frac{c}{4\pi nc} \nabla^2 \underline{A} \times (\nabla \times \underline{A} + \underline{B}_o) + \frac{\underline{J}}{ne} \times [(\nabla \times \underline{A}) + \underline{B}_0] + \frac{c^2 \eta}{4\pi} \nabla^2 \underline{A} \right\}_t . \qquad (8)$$

The right hand side of Eq. (8) requires a decomposition into longitudinal and transverse parts. In special cases (e.g., one-dimensional cases or Hewett's axisymmetric model) this can be done geometrically. However, in general, and for the non-axisymmetric long layer problems that we wish to examine, geometric decomposition is not possible.

Equation (8) can be written as

$$\frac{\partial \underline{A}}{\partial t} - c\nabla\phi = \frac{c}{4\pi ne} \nabla \underline{A} \times (\nabla \times \underline{A} + \underline{B}_o) + \frac{\underline{J}}{ne} \times [(\nabla \times \underline{A}) + \underline{B}_o] + \frac{c^2 \eta}{4\pi} \nabla^2 \underline{A} \qquad (9)$$

where ϕ represents a potential such that $\underline{E}_\ell = -\nabla\phi$. This equation now has a form somewhat similar to that of the Navier-Stokes equation for incompressible flow:

$$\frac{\partial \underline{u}}{\partial t} + \nabla P = -\underline{u} \cdot \nabla \underline{u} + \nu \nabla^2 \underline{u} . \qquad (10)$$

A critical difference between the two equations lies in the boundary conditions. In Eq. (9), the potential ϕ and one component of the vector potential, $\underline{A}$, are known at the boundaries. In the Navier-Stokes equation, the pressure at the boundary is generally unknown, while both components of the flow velocity, $\underline{v}$, are specified. Therefore, some methods used in solving the two-dimensional Navier-Stokes equation[2,3] may be applied to Eq. (10), but not without significant modifications to handle the different boundary conditions. The fact that the scalar potential is specified on the boundary in the quasineutral equation makes it a straightforward process to obtain ϕ from a Poisson equation (as opposed to the fluid case where the boundary condition must be predicted to solve a Poisson equation for P). Writing the right-hand side of Eq. (9) as $\mathcal{F}(A)$, we have, in two dimensions,

$$\frac{\partial A_x}{\partial t} - c\nabla_x\phi = \mathcal{F}_x(\underline{A}) \tag{11a}$$

$$\frac{\partial A_y}{\partial t} - c\nabla_y\phi = \mathcal{F}_y(\underline{A}) \tag{11b}$$

$$\nabla^2\phi = -\nabla\cdot\underline{\mathcal{F}}(\underline{A}) \ . \tag{11c}$$

Equations (11a,b,c) form a non-linear system of three equations in three unknowns, which must be solved simultaneously. Equations (11a and 11b) are non-linear in that they have products of $\underline{A}_x$ and $\underline{A}_y$, but neither contains a term like A_x^2 or A_y^2. These equations may each be advanced in a Crank-Nicolson scheme. This forms a predictor-corrector method for the advance of all three quantities. For the m-th of M iterations we have

$$\frac{A_x^{n+1,m}-A_x^{n}}{\Delta t} = \frac{c}{2}\left(G_x\phi^{n+1,m} + G_x\phi^{n}\right) + \frac{1}{2}\left(\mathcal{F}_x^{n+1,m}(\underline{A}) + \mathcal{F}_x^{n}(\underline{A})\right) \quad (12a)$$

$$\frac{A_y^{n+1,m}-A_y^{n}}{\Delta t} = \frac{c}{2}\left(G_y\phi^{n+1,m} + G_y\phi^{n}\right) + \frac{1}{2}\left(\mathcal{F}_y^{n+1,m}(\underline{A}) + \mathcal{F}_y^{n}(\underline{A})\right) \quad (12b)$$

$$L\phi^{n+1,m} = -D\mathcal{F}^{n+1,m}(\underline{A}) \; . \quad (12c)$$

L, D, and G are the finite difference approximations for the Laplacian, divergence, and curl, respectively. The operator L should be such that

$$L\phi = DG\phi \; . \quad (13)$$

With interlaced grids, using four-point operators to represent the derivatives in the gradient operators, i.e.,

$$\left.\frac{\partial\phi}{\partial x}\right|_{i+\frac{1}{2},j+\frac{1}{2}} \rightarrow \frac{\phi_{i+1,j+1}+\phi_{i+1,j-1}-\phi_{i-1,j+1}-\phi_{i-1,j-1}}{2\Delta x}) \; . \quad (14)$$

Eq. (13) implies that L be defined by

$$L\phi \equiv \frac{\phi_{i+1,j+1}+\phi_{i+1,j-1}+\phi_{i-1,j+1}+\phi_{i-1,j-1}-4\phi_{i,j}}{2(\Delta x)^2} \; . \quad (15)$$

Because all three of Eqs. (12) involve the solution of a large matrix equation, the method is totally impractical for large M. It is assumed that $M \leq 2$ wil be sufficient. While the time requirements for this type of solution might be prohibitive in a fluid code, the largest fraction of time used by a hybrid code is expected to be in the particle mover. Hopefully, this will allow the flexibility to solve a system of equations such as (12). If a technique such

as orbit averaging is used for the particle mover, then the time constraints on the field solver will be reduced further.

The most attractive way to solve Eqs. (12) appears to be the ICCG (incomplete Cholesky conjugate gradient) method, because of the large variation in the magnitude of the diagonal elements from the plasma to the vacuum regions.[4] The first predictor steps should require a relatively small number of iterations, as it would be unnecessary to demand a small residual in the predictor solution.

Once $\underline{A}$ and ϕ have been advanced, the new values for $\underline{E}$ and $\underline{B}$ can be obtained from

$$\underline{B}^{n+1} = \nabla \times \underline{A}^{n+1} + \underline{B}_o$$

$$\underline{E}^{n+1} = \frac{1}{c} \underline{\mathcal{F}}(\underline{A})^{n+1} .$$

These fields can then be used to advance the particles with the standard techniques.

REFERENCES

1. D. W. Hewett, "A Global Method of Solving the Electron-Field Equations in a Zero-Inertia-Electron-Hybrid Plasma Simulation Code", submitted to J. Comp. Phys.
2. A. J. Chorin, "Numerical Solutions of the Navier-Stokes Equations", Math. of Comp. 22, pp. 745-762 (1968).
3. A. I. Shestakov, "A Hybrid Vortex-ADI Solution for Flows of Low Viscosity", J. Comp. Phys. 31, pp. 313-334 (1979).
4. D. S. Kershaw, "The Incomplete Cholesky-Conjugate Gradient Method for the Iterative Solution of Systems of Linear Equations", J. Comp. Phys. 26, pp. 43-65 (1978).

D. Effects of Intrinsic Orbital Stochasticity on Resonant Microinstability (Bruce Cohen and Alex Friedman)

Complex inhomogeneous equilibria can exhibit intrinsic stochasticity; i.e. certain classes of particles have stochastic orbits. An illustrative and familiar example arises in simple mirror systems. For axisymmetric mirror machines particle energy $\mathcal{E}$ and canonical angular momentum P_θ are conserved in the absence of turbulence or other perturbations that break azimuthal symmetry and introduce explicit time dependence. When the Larmor radius is small compared to the magnetic scale lengths, the magnetic moment μ and the longitudinal action J are approximate (or adiabatic) invariants. The magnetic moment can experience changes when somewhere along the particle trajectory the cyclotron frequency or its harmonic equals a harmonic of the axial bounce frequency. For changes in μ from one bounce to another that are unrelated, the particle motion remains orderly and deterministic, but the changes in μ as the particle passes through resonance on successive axial transits can be viewed as a stochastic process. Neighboring stochastic orbits in the phase space of μ, J, and their conjugate angles appear to diverge exponentially in time when averaged over many bounce periods.

What effects does intrinsic orbital stochasticity have on microinstability? Intrinsic stochasticity is not collective in nature; the orbit separation of various sets of neighboring particles in phase space is uncorrelated when viewed over many bounce periods. Furthermore, stochasticity does not influence the moments of the distribution function and, in particular, does not alter any free energy possibly available nor the macroscopic charge densities and currents. Therefore, we conjecture that the effects of stochasticity on microinstability may be weak provided that the equilibrium orbits are not too much distorted. The following discussion fills in the details of this argument and supports its conclusion.

For simplicity we assume that the linear growth rate of an unstable mode and the stochasticity rate (orbital separation rate) are both much smaller than the mode frequency, cyclotron and bounce frequencies. Upon integrating the Vlasov equation along its characteristics, i.e. performing the integral

$$\delta f \propto \int_{-\infty}^{t} dt' \exp\ [iky(t') - i\omega t'] \qquad (1)$$

in slab coordinates, denominators appear with resonance condition

$$\Delta\omega \equiv \omega - \ell\bar{\omega}_{ci}(J,\mu,X) + 2p\omega_b(\mu) + kV_d(\mu) = 0 \quad , \tag{2}$$

where $\bar{\omega}_{ci}$ is the average cyclotron frequency, ω_b is the bounce frequency, V_d is the drift velocity, and X is the guiding center position (see Smith, Byers, and LoDestro UCRL-82674).

We now presume that the adiabatic invariants μ and J begin to slowly diverge due to intrinsic stochasticity. Hence, $\Delta\omega = \Delta\omega(t)$ and a particle will cease to be resonant when

$$\int_0^{\tau_s} dt' \; \Delta\omega(t') = \theta(\pi) \quad ,$$

which defines τ_s and relates it to the stochasticity rate. Over the time period τ_s the particle can do work on the wave and vice versa. Meanwhile, however, accompanying the loss of resonance for one particle, there is an equal probability that a neighboring particle in phase space is coming into resonance. Resonance again persists over a time period of order τ_s. The <u>linear</u> perturbations of the resonant particles will add, and the linear dielectric response will be largely unaffected by stochasticity. The crux of the argument is that with stochastic orbits we expect an equal flux of particles into and out of resonance at any point on the separatrix between resonant and nonresonant particles but the wave-particle interaction while in resonance is unaffected. <u>Nonlinear</u> aspects of the wave-particle interaction are decidedly affected when intrinsic stochasticity limits the duration of resonance, essentially because nonlinear effects associated with particles coming in and out of resonance are not simply additive.

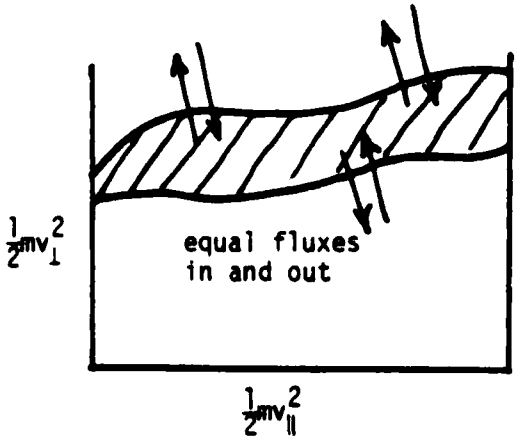

Cartoon of separatrix for particles resonant with an ion cyclotron flute mode (see Smith <u>et. al.</u>, UCRL-82674) showing fluxes of stochastic particles.

When τ_s becomes so short that τ_s^{-1} is comparable to the smallest characteristic frequency helping to determine the resonance condition, Eq. (2), then the resonance is destroyed. In this case the particle will interact simultaneously with many of the bounce harmonics, and there is no resonance with any one particular bounce harmonic. Thus, stochasticity will profoundly influence the linear aspects of resonant microinstability when the stochasticity rates becomes comparable to the characteristic frequencies.

Random collisions have a very different effect on microinstability. Use of the simplest Krook model yields the following modification to the resonant denominators appearing in δf,

$$\Delta\omega = \omega - \ell\bar{\omega}_{ci} + 2p\omega_b + kV_d + i\nu_c \quad . \tag{3}$$

In the absence of collisions, $\text{Im}\,\Delta\omega = \text{Im}\omega = \gamma$, the linear growth rate. With collisions, $\text{Im}\,\Delta\omega = \gamma + \nu_c$. Thus, collisions will have a significant effect when $\nu_c = \mathcal{O}(\gamma)$. Physically, collisions produce a real diffusion of particles in phase space and destroy $\mathscr{E}$ and P_θ conservation, as well as alter μ and J. Wave growth is necessarily accompanied by momentum and energy exchange with resonant particles. Therefore, at the point when the collision rate becomes large enough to influence the energy and momentum exchange of the resonant particles interacting with the wave, microinstability would be significantly altered.

To illustrate collisional effects, consider the force on a resonant particle due to a wave in the presence of randomizing collisions,

$$\frac{d}{dt}\,\delta v = \frac{F}{m}\,e^{-i\Delta\omega t} + \text{c.c.} \quad - \nu_c\,\delta v \quad , \tag{4}$$

where δv is the perturbed velocity in the frame of the unperturbed particle motion, F is the amplitude of the force, and $\Delta\omega$ might be given by $\Delta\omega = \omega - kv$, Eq. (2), or one's favorite resonance condition. The solution of Eq. (4) is

$$\delta v = \frac{Fm^{-1}}{-i\Delta\omega + \nu_c}\,e^{-i\Delta\omega t} + \text{c.c.} = \frac{Fm^{-1}}{\sqrt{\Delta^2 + (\nu_c + \gamma)^2}}\,e^{-i\Delta\omega t + i\delta} + \text{c.c.} \quad , \tag{5}$$

where $\cos\delta = (\nu_c+\gamma)/\sqrt{\Delta^2 + (\nu_c+\gamma)^2}$, $\Delta \equiv \mathrm{Re}\ \Delta\omega$, and any initial transient has been allowed to damp away. It is obvious from this simple expression that the energetics of the wave-particle interaction are significantly affected when ν_c becomes comparable to γ.

It appears that there can be considerable stochasticity without there being much effect on the linear aspects of resonant microinstability. In simulations such as Friedman's three-dimensional linearized simulations of field-reversing rings and mirrors, intrinsic stochasticity of particle orbits is often observed. Based on the arguments presented here, if particle statistics in the simulation are very good, but not economically unmanageable, so that there is the necessary cancellation of the stochastic particle flux into and out of resonance with the wave, then one expects that Friedman's code could investigate resonantly driven instabilities even in the low growth rate regime. Obviously, the higher the growth rates of the modes under investigation the less perfect the cancellation of stochastic particle flux need be and the fewer simulation particles necessary. Remaining to be done is the quantitative assessment of the particle statistics requirements for simulation of modes in the regime where the stochasticity rate exceeds the instability growth rate.

We thank John Finn and Jim Albritton for illuminating discussions of these issues, and Brendan McNamara for posing the problem.

E. Effects of Numerical Dissipation on Simulation of Fast and Slow Space-Charge Waves

Bruce I. Cohen

The introduction of backward time-differencing in the numerical solution of either ordinary or partial differential equations with time dependence can lead to frequency-dependent numerical dissipation. This can be exploited and provide a means of performing digital filtering in numerical simulations of time-dependent phenomena [1-3]. In Ref. 1 digital time filtering is combined with an implicit differencing scheme to achieve damping of high frequency waves in an unconditionally stable algorithm that allows use of large time steps. This approach is suitable for solution of fluid equations and linearized kinetic equations, e.g., the drift-kinetic equation [1]. Unfortunately, implicit solution of nonlinear kinetic equations frequently leads to inversion of large non-sparse matrices[4]. This is particularly true of particle codes, and thus the implicit methods described in Ref. 1 have not been applied to particle simulations. Nevertheless, digital filtering has been frequently used in particle codes to damp unwanted high frequency modes and recently has been combined with a new technique called orbit-averaging to allow the use of a large time-step in the solution of the self-consistent fields [2].

An interesting and important question has been raised regarding the use of numerical algorithms with artificial dissipation added. Because negative energy modes in plasmas or in other dielectric media can be destabilized by dissipation, it is wondered whether numerical dissipation can artificially destabilize negative energy modes. The following discussion demonstrates that numerical dissipation can in fact destabilize negative energy modes, but that with some ingenuity dissipative algorithms can be devised that damp both positive and negative energy modes increasingly as the mode frequency increases.

The simplest model admitting positive and negative energy modes is that of a cold, unmagnetized, drifting plasma. The infinite homogeneous plasma dispersion relation for plasma waves becomes

$$(\omega - ku_0)^2 = \omega_p^2 \quad , \tag{1a}$$

with solutions

$$\omega = ku_0 \pm \omega_p \quad , \tag{1b}$$

where u_0 is electron drift speed relative to an immobile neutralizing ion background, k is the wavenumber, and ω_p is the electron plasma frequency. The +(-) sign in Eq. (1b) corresponds to the fast (slow) beam mode, which has positive (negative) wave energy. As we shall illustrate, the slow wave can be driven unstable by dissipation.

Consider the one-dimensional particle simulation algorithm given by

$$v^{n+1/2} = v^{n-1/2} - eE^n\Delta t/m \tag{2a}$$

$$x^{n+1} = x^n + v^{n+1/2}\Delta t \tag{2b}$$

$$(1-\epsilon)\frac{\partial}{\partial x}E^n + \epsilon\frac{\partial}{\partial x}E^{n-1} = -4\pi e(n^n - n_0) \tag{2c}$$

where X and V are electron positions and velocities, E is the electric field, n_0 is the unperturbed homogeneous background number density, the superscript n denotes the time level, and ε is a centering parameter ($\varepsilon = 0$ is perfectly time-centered). To analyze the system of equations given in Eq. (2), we linearize, use the relation

$$n^{(1)} = - n_0 \partial X^{(1)}/\partial x \quad , \tag{3}$$

employ the Fourier representation

$$E = \tilde{E} \exp(- i\omega t + ikx) + c.c.$$

for all perturbed quantities, and define

$$\lambda \equiv \exp(- i\omega\Delta t/2 + iku_0\Delta t/2)$$

to obtain

$$(\lambda - \lambda^{-1})\tilde{V} = - e\Delta t\tilde{E}/m \tag{4a}$$

$$(\lambda - \lambda^{-1})\tilde{X} = \tilde{V}\Delta t \tag{4b}$$

$$(1 - \varepsilon + \varepsilon e^{i\omega\Delta t})\tilde{E} = 4\pi e n_0 \tilde{X} \quad . \tag{4c}$$

The dispersion relation for this system of equations is easily determined:

$$(1 - \varepsilon + \varepsilon e^{i\omega\Delta t})(\lambda - \lambda^{-1})^2 + \omega_p^2\Delta t^2 = 0 \quad . \tag{5}$$

For $|\omega\Delta t| << 1$, $e^{i\omega\Delta t} \approx 1 + i\omega\Delta t$ and Eq. (5) has solution

$$\lambda^2 \approx 1 \pm i\alpha - \frac{\alpha^2}{2} \pm \alpha\varepsilon\frac{\omega\Delta t}{2} + \ldots \quad , \tag{6}$$

where

$$\hat{\alpha} \equiv \omega_p \Delta t/(1 + \varepsilon^2\omega^2\Delta t^2)^{1/2} << 1 \quad .$$

From Eq. (6) and the definition of λ, we deduce

$$\text{Re } \omega \approx ku_0 \mp \omega_p/(1 + \varepsilon^2\omega^2\Delta t^2)^{1/2} \tag{7a}$$

and

$$|\lambda^2| \approx 1 \pm \frac{\varepsilon\omega\omega_p\Delta t^2}{2(1 + \varepsilon^2\omega^2\Delta t^2)^{1/2}} \quad .$$

One concludes from Eqs. (7a) and (7b) that the fast mode is damped and the slow wave destabilized for $\varepsilon > 0$ and $ku_0 \pm \omega_p > 0$. Furthermore, $|\text{Im } \omega| \approx (1/2)\varepsilon\omega_p\Delta t|\text{Re } \omega|$, i.e., the damping and growth rates are frequency dependent. The same sorts of results are obtained with use of

$$\frac{\partial E^n}{\partial x} = -(1 + \varepsilon)\, 4\pi e(n_n - n_0) - \varepsilon \frac{\partial}{\partial x} E^{n-1} \tag{8}$$

in place of Eq. (2c).

A useful interpretation of the effects of finite ε in Eqs. (2c) and (8) can be given by observing that these equations can be cast in a form equivalent to

$$\frac{\partial}{\partial x}\left(\frac{\partial E}{\partial t} + 4\pi J + 4\pi\sigma E\right) = 0 \quad , \tag{9}$$

where J is the plasma current and σ is an electrical conductivity representing the interaction of the plasma with a resistive background.

For $|\sigma/\omega| << 1$, the dispersion relation given in Eq. (1) becomes

$$\omega = ku_0 \pm \frac{\omega_p}{\left[1 + \frac{(4\pi\sigma)^2}{(ku_0 \pm \omega_p)^2}\right]^{1/2}} \left(1 - \frac{i\pi 2\sigma}{ku_0 \pm \omega_p}\right) \quad . \tag{10}$$

For $\sigma > 0$ and $ku_0 > \omega_p$, the slow wave is unstable and the fast wave is damped. This is the underlying physical mechanism for the resistive wall amplifier[5]. The structure of Eq. (10) is very similar to Eqs. (7a) and (7b) and permits an identification of a frequency-dependent numerical *conductivity*.

An alternative algorithm to that given in Eq. (2) is

$$(1 - \varepsilon)(v^{n+1/2} - v^{n-1/2}) + \frac{1}{2}\varepsilon(v^{n+1/2} - v^{n-3/2}) = -eE^n\Delta t/m \tag{11a}$$

$$x^n - x^{n-1} = v^{n-1/2}\Delta t \tag{11b}$$

$$\frac{\partial E^n}{\partial x} = -4\pi e(n^n - n_0) \quad . \tag{11c}$$

With $\varepsilon > 0$, the time derivative of the velocity is backwards-differenced with respect to the electric field in Eq. (11a). Employing the definitions and Fourier representation introduced earlier, we linearize and obtain the bi-cubic dispersion relation

$$\lambda^2(\lambda^2 - 1)^2 - \frac{\varepsilon}{2}(\lambda^2 - 1)^3 + \omega_p{}^2\Delta t^2\lambda^4 = 0 \quad . \tag{12}$$

For $\omega_p\Delta t, << 1$ Eq. (12) has one branch with solution given by $\lambda^2 = -\varepsilon/(2 - \varepsilon)$, which is damped for $\varepsilon < 1$. For $\omega_p\Delta t$, $|\varepsilon| << 1$ the remaining solutions are

$$\lambda^2 = 1 \mp \omega_p\Delta t\,(1 \mp i\varepsilon\omega_p\Delta t/4) - \frac{\omega_p{}^2\Delta t^2}{2}(1 \mp i\varepsilon\omega_p\Delta t/4)^2 + \ldots \quad ,$$

or equivalently

$$\omega \approx ku_0 \pm \omega_p - i\varepsilon\omega_p{}^2\Delta t/4 \tag{13a}$$

$$|\lambda^2| \approx 1 - \varepsilon\omega_p{}^2\Delta t^2/4 < 1 \tag{13b}$$

for $\varepsilon > 0$. Thus, both fast and slow beam modes are damped. The damping rate is $\varepsilon\omega_p^2\Delta t/4$ and vanishes in the limit that $\varepsilon \to 0$. This algorithm has an effective numerical conductivity which is positive for the fast mode and negative for the slow mode.

For $\omega_p\Delta t >> 1$, Eq. (12) becomes

$$(1 - \varepsilon/2)\lambda^4 \approx - \omega_p{}^2\Delta t^2\lambda^2$$

for one branch of solutions; and thus $|\lambda| \approx \omega_p\Delta t/(1 - \varepsilon/2)^{1/2} > 1$ for $\varepsilon < 2$, i.e., the algorithm is numerically unstable for large time steps. The remaining solutions of Eq. (12) are given by

$$\lambda^2 = \frac{1}{2\omega_p{}^2\Delta t^2} \pm \frac{1}{2}\left(\frac{1}{\omega_p{}^4\Delta t^4} - \frac{2\varepsilon}{\omega_p{}^2\Delta t^2}\right)^{1/2}$$

for $\omega_p^2\Delta t^2 >> \varepsilon, 1$ and are heavily damped ($|\lambda^2| << 1$).

For $\varepsilon = 0$ and general value of $\omega_p\Delta t$, Eq. (12) simplifies to the dispersion relation for the conventional leap-frog algorithm,

$$(\lambda^2 - 1)^2 + \omega_p{}^2\Delta t^2\lambda^2 = 0 \quad ,$$

with solution

$$\sin^2(ku_0 - \omega)t = \omega_p{}^2\Delta t^2/4 \quad ,$$

which is stable for $\omega_p \Delta t \leq 2$. For small but finite ε and $\alpha \equiv \omega_p \Delta t$ very nearly equal to 2, the dispersion relation in Eq. (12) can be expanded for small perturbations $\delta\varepsilon$ and $\delta\alpha$, with respect to $\varepsilon = 0$ and $\alpha = 2$,

$$D(\lambda^2; \varepsilon, \alpha) \approx D(\lambda^2 = -1; \varepsilon = 0, \alpha = 2) + \delta\varepsilon \left.\frac{\partial D}{\partial \varepsilon}\right|_{\varepsilon=0} + \delta\alpha \left.\frac{\partial D}{\partial \alpha}\right|_{\alpha=2} = 0 \quad , \qquad (14)$$

where $D(\lambda^2; \varepsilon, \alpha)$ is given by Eq. (12) and $D = 0$ at $\lambda^2 = -1$ for $\varepsilon = 0$ and $\alpha = 2$. Equation (14) then yields

$$\delta\alpha = -\delta\varepsilon \left(\frac{\partial D}{\partial \varepsilon} \Big/ \frac{\partial D}{\partial \alpha}\right)\Big|_{\varepsilon = 0,\ \alpha = 2,\ \lambda^2 = -1} = -\delta\varepsilon \quad . \qquad (15)$$

This demonstrates that the introduction of a small amount of biasing, $0 < \delta\varepsilon \ll 1$, shifts the stability boundary of the algorithm to slightly <u>smaller</u> values of $\omega_p \Delta t$.

A. B. Langdon has contributed the valuable observation that the backwards biasing in Eq. (11a) occurs in a Lagrangian equation and is invariant under a Galilean transformation. Thus, dissipation is introduced in a way that is independent of reference frame; and artificial destabilization of a beam mode should not be expected when a drift is added. In contrast, the backwards biasing in the first algorithm, Eq. (2), is performed in the field equation, which is Eulerian in nature. The resulting effects are not invariant under a Galilean transformation, and the mischief caused in the slow beam mode is not so surprising.

Birdsall has commented that biasing the field equation in Eq. (2c) is equivalent to changing the dielectric medium in such a way that ω_p^2 becomes complex. This results in the destabilization described in Eq. (10).[5]

However, with the biasing indicated in Eq. (11a), the equation of motion is changed in a purely dissipative way, effectively

$$\frac{dv}{dt} \rightarrow \frac{dv}{dt} - \varepsilon' \frac{d^2v}{dt^2} = - eE/m$$

where $\varepsilon' = \varepsilon\Delta t/2 > 0$; and upon Fourier analyzing, $(\omega - ku_0) \rightarrow [\omega - ku_0 + i\varepsilon'(\omega - ku_0)^2]$. This scheme should damp all waves for small values of $\omega_p\Delta t$.

One concludes that digital time filtering need <u>not</u> lead to artificial destabilization of negative energy waves. Algorithms can be devised which damp both positive and negative energy waves as an increasing function of mode frequency and time step. However, in an explicit differencing scheme, the backwards biasing of the difference equations necessary to achieve time filtering is likely to make the time-step constraint for numerical stability slightly more stringent.

I am pleased to acknowledge many helpful discussions with Bill Fawley, Bruce Langdon, and C. K. Birdsall, and am indebted to Brendan Godfrey for posing the problem. This work was performed under the auspices of the U.S. Department of Energy at Lawrence Livermore Laboratory under contract number W-7405-ENG-48.

References

1. T. L. Crystal, J. Denavit, and C. E. Rathman, "On Numerical Solutions of the Vlasov Equation with Filtering in Time," comments Plas. Phys. Cont. Fusion 5, 17 (1979).

2. B. I. Cohen, T. A. Brengle, D. B. Conley, and R. P. Freis, "An Orbit-Averaged Particle Code," Lawrence Livermore Laboratory Report, UCRL-82832 (June 1979). Accepted for publication in J. Comp. Phys.

3. W. M. Fawley and C. K. Birdsall, "Digital Filtering in Time," Third Quarter Progress Report on Plasma Theory and Simulation (July-Sept., 1979), Electronics Research Laboratory, U.C. Berkeley, p. 57.

4. A. B. Langdon, "Analysis of the Time Integration in Plasma Simulation," J. Comp. Phys. 30, 202 (1979).

5. C. K. Birdsall, G. R. Brewer, and A. V. Haeff, "The Resistive-Wall Amplifier," Proc. IRE, 41, 865 (1953).

F. Orbit Averaging: A Technique for Filtering out High Frequency Waves and Fluctuations.

Vincent Thomas (Prof. C. K. Birdsall and B. I. Cohen)

A technique first used by Cohen et al. (Ref. 1), referred to as orbit averaging, has been written for use in ES1, our 1-D electrostatic code in an attempt to filter out high frequency electron waves and leave the low frequency motion of both particle electrons and ions and the associated self-consistent electric field. In this method, the electrons and ions are advanced on their respective time scales, but the fields are solved for only on the ion time scale. The field solver uses a time filtered source term, the charge density, in order to filter out the high frequency phenomena. For all cases considered here, the time filtering consists of an equally weighted average. The flow chart is shown in Fig. 1. Also shown is the scheme for moving from one macro time step to the next macro time step. The velocities of the electrons are known at the short hash marks, and the velocities of the ions are known at the long hash marks. The fields are solved for at the dots. After the fields are solved for, the electrons and ions are moved from $N\Delta T-\frac{1}{2}\Delta t_i$ to $(N+1)\Delta T-\frac{1}{2}\Delta t_i$ and from $N\Delta T-\frac{1}{2}\Delta t_e$ to $(N+1)\Delta T-\frac{1}{2}\Delta t_e$, respectively. The electrons must be moved in a series of short steps to satisfy $\omega_{pe}\Delta t_e < 2$. The electron time step and the ion time step will be referred to as the micro step and the macro time step, respectively.

In attempting to introduce some flexibility one may introduce various biasing parameters. The first of these is in the field solver where one uses Eq. (1)

$$-\varepsilon\nabla^2\phi^{N+1} - (1-\varepsilon)\nabla^2\phi^{N} = 4\pi e(n_i(x) - \bar{n}_e(x)) \qquad (1)$$

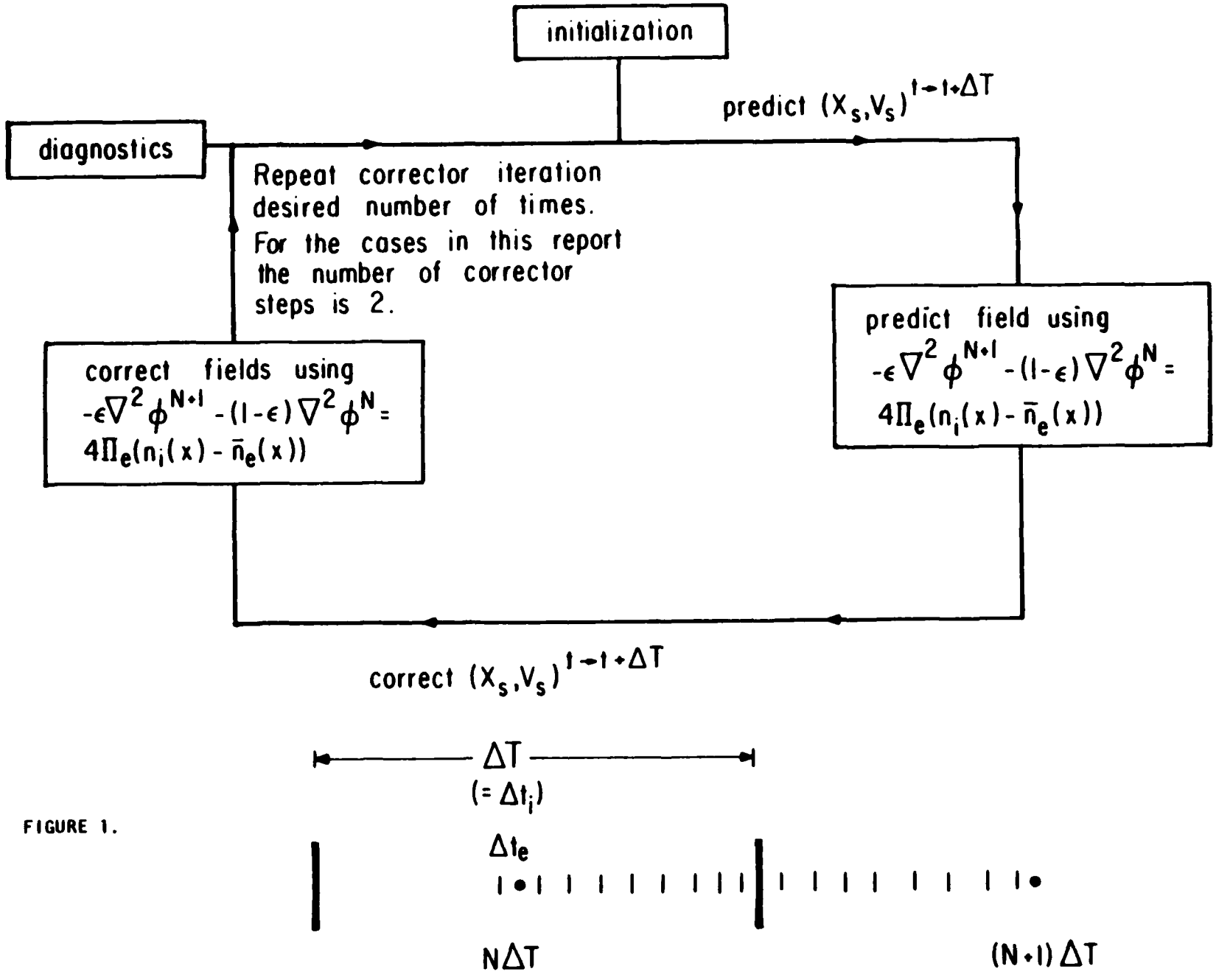
initialization
predict $(X_s, V_s)^{t \to t+\Delta T}$
diagnostics
Repeat corrector iteration desired number of times. For the cases in this report the number of corrector steps is 2.
predict field using
$-\epsilon\nabla^2\phi^{N+1} - (1-\epsilon)\nabla^2\phi^N =$
$4\Pi_e(n_i(x) - \bar{n}_e(x))$
correct fields using
$-\epsilon\nabla^2\phi^{N+1} - (1-\epsilon)\nabla^2\phi^N =$
$4\Pi_e(n_i(x) - \bar{n}_e(x))$
correct $(X_s, V_s)^{t \to t+\Delta T}$
ΔT
$(= \Delta t_i)$
Δt_e
$N\Delta T$
$(N+1)\Delta T$

FIGURE 1.

When ω_{ce} was larger than ω_{pe}, simulations of a cold plasma produced clear cut oscillations, with frequencies at the lower hybrid frequency. Runs were made for $\omega_{ce} = 5$ and 2.5 with $\omega_{pe} = 1,2,3$, and 4. For ω_{ce} less than ω_{pe}, the oscillations were not as clear, and energy conservation was poor.

Figure 2 shows an ω vs k diagram for a particular set of parameters. The formula used to calculate the theory curve means using the usual finite $k\Delta x$ correction appropriate to linear weighting,

$$\omega(k\Delta x) = \omega_{pi}(k\Delta x)\Big/\sqrt{1+\left(\frac{\omega_{pe}(k\Delta x)}{\omega_{ce}}\right)^2} \quad . \qquad (2)$$

The difference between theory and simulation is only significant for modes 14 and 15. No k-space smoothing was used in any of these simulations and so some of the simulations were of poor quality. The frequencies were clearly visible in the electrostatic energy history plots in all cases, as the simulations were done by exciting only one mode at a time. The modes were excited with a sinusoidal perturbation in ion and electron positions.

For cold lower hybrid waves, it was necessary to use ε larger than 1 to achieve satisfactory energy conservation. Using ε greater than 1 amounts to an interpolation of the potential at a time later than the $(N+1)^{th}$ macro time step. For $0.6 < \varepsilon < 2.5$ the period of the hybrid oscillations observed was within a few percent of the expected period, assuming the usual $k\Delta x$ correction due to linear weighting. Figure 3 shows the variation of total energy vs. ε, with large loss for small ε. The field energy and the kinetic energies damp at approximately the same rate; this means

to solve for ϕ^{N+1}. Here N+1 designates the $(N+1)^{th}$ macro time step which, in general, could be different from the ion time step; for all work done here the macro time step is equal to the ion time step. $n_i(x)$ is the ion charge density at macrotime steps; $\bar{n}_e(x)$ is the electron charge density averaged over all of the micro time steps from $N\Delta T-\frac{1}{2}\Delta t_e$ to $(N+1)\Delta T-\frac{1}{2}\Delta t_e$ (see Fig. 1).

Another biasing parameter can be introduced in the electron mover. For the predictor step, the electrons are moved by $E=-\nabla\phi^N$, which is taken to be constant in time. For the corrector iteration, one could use an E(t) which is linearly interpolated from the $(N)^{th}$ to the $(N+1)^{th}$ macro time step, as

$$E(t) = -(1-bias2)\nabla\phi^N + (t-N\Delta T)(1+bias2)\left(\frac{-\nabla\phi^{N+1}-\nabla\phi^N}{\Delta T}\right)$$

where ΔT is the macro time step. In the simulations presented in this report bias2=0. The effects of the parameter bias2 will be commented on at a later time.

The primary advantage of orbit averaging is the reduction in the number of particles needed for a simulation [1]. This is possible because the high frequency part of the thermal spectrum is removed by this simulation scheme.

Simulations have been made for cold and warm magnetized plasmas and for warm unmagnetized plasmas using real mass ratios (e.g., $m_i/m_e=1836$). Preliminary results have been encouraging. Results of the three different cases will be discussed separately, with the results of the warm unmagnetized simulations being deferred until a later date.

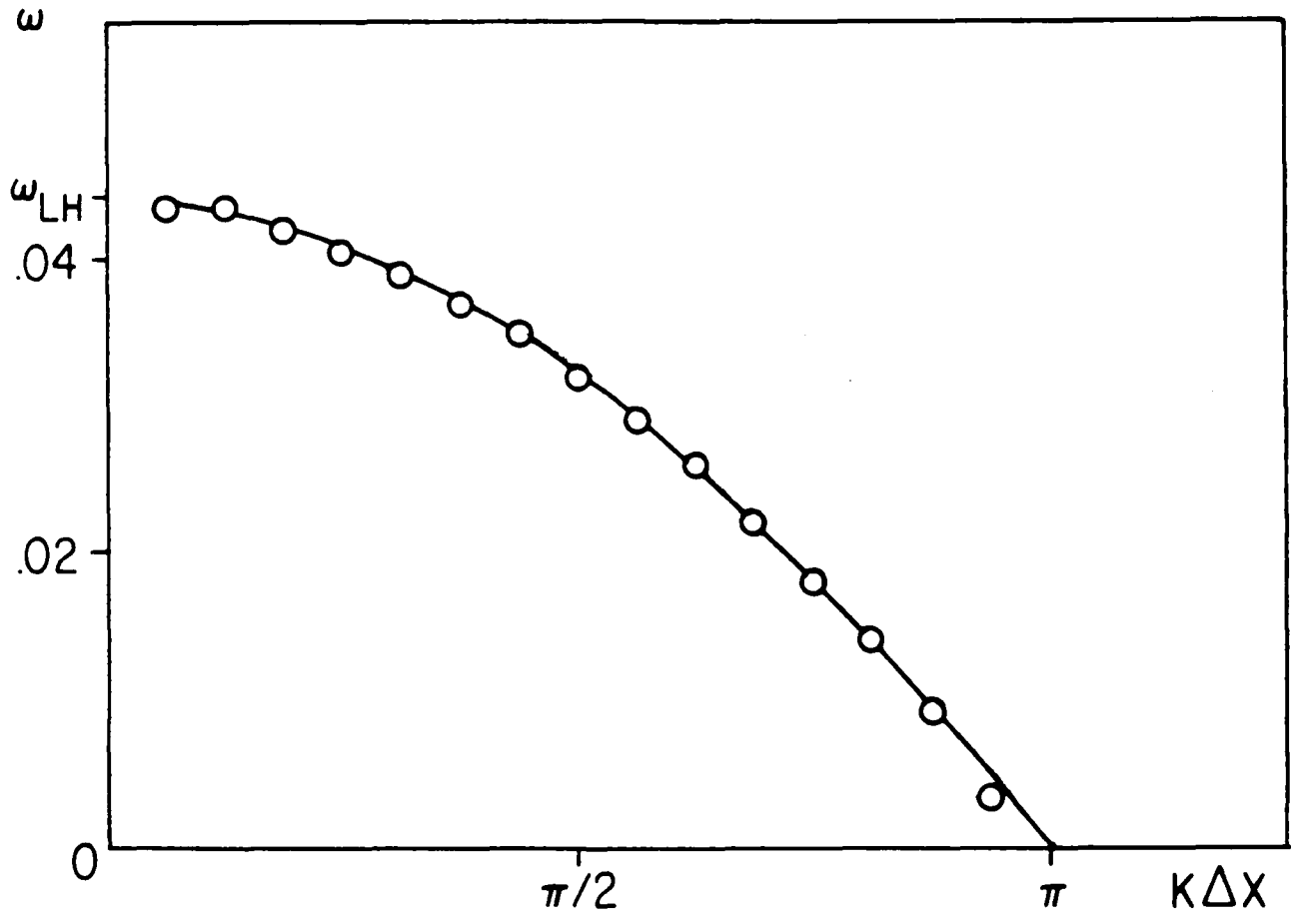

FIG. 2 Frequencies of oscillations for a cold magnetized plasma. The parameters were: $\omega_{pe} = 2.0$, $\omega_{ce} = 5.0$, $m_i/m_e = 1760$, the electron time step was $\Delta t_e = .03$, the ion time step $\Delta t_i = 3.0$, there are 512 electrons and 512 ions, NG = 32, and the amplitude of the sinusoidal perturbation is $\sim 10^{-6}$ of a particle separation. The bias parameter ε is equal to 1. The curve represents theory, the points simulation data. Linear weighting was used.

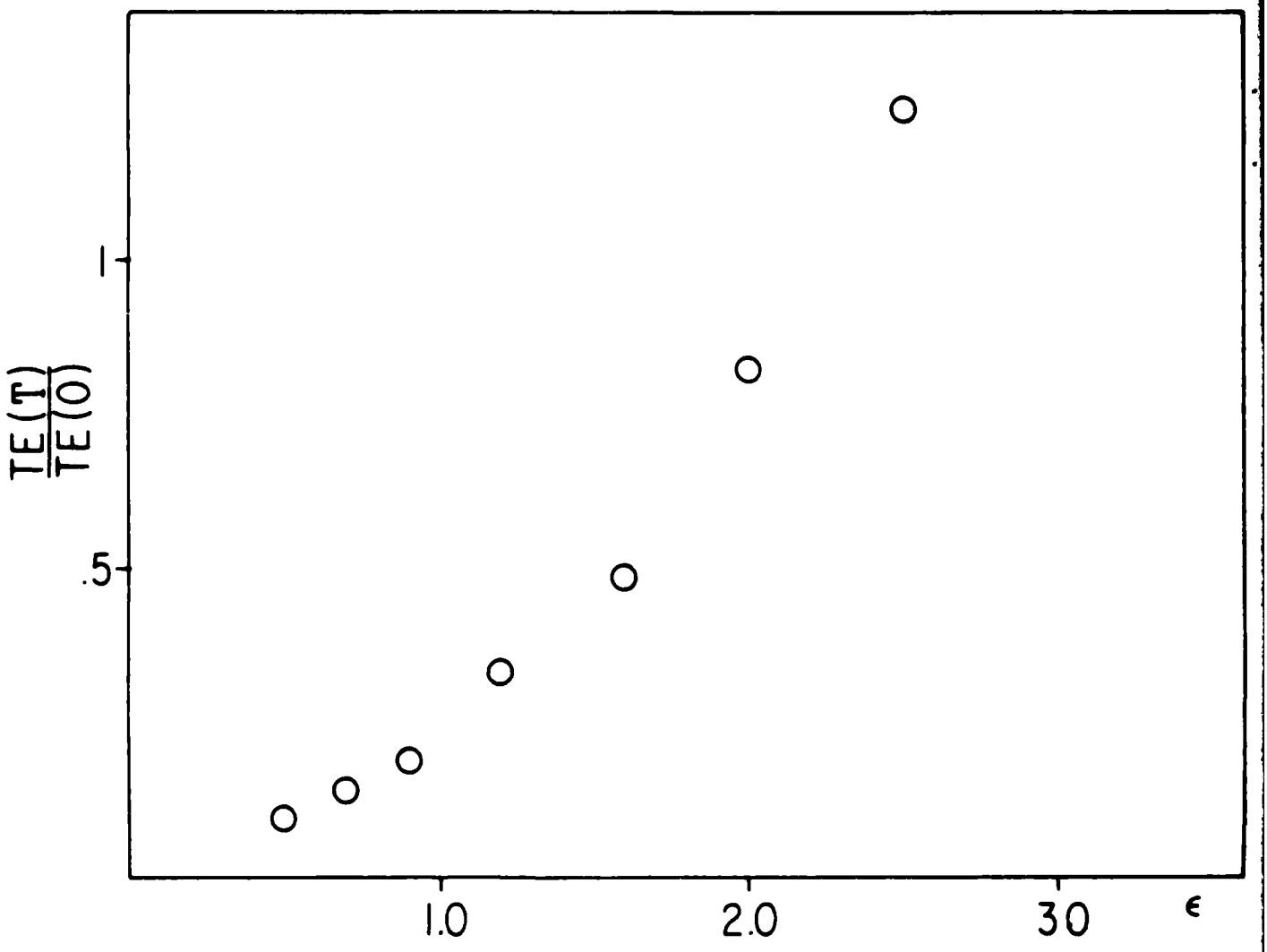

FIG. 3 Dependence of energy conservation on bias parameter ϵ. For these simulations $\Delta t_e = 3.0$, $\Delta t_i = 3.0$, $m_i/m_e = 1836$, $\omega_{pe} = 2.0$, $\omega_{ce} = 5.0$, NG = 32, L = 32, and there are 512 cold electrons and ions. The amplitude of the initial sinusoidal perturbation was $\sim 10^{-6}$ of a particle separation. T.E.(T) and T.E.(0) are the total energies at $T(=\omega_{pe}t=300)$ and at t = 0, respectively.

that the low frequency energy (e.g., field energy at $\omega \approx \omega_{LH}$) damps at the same rate as the higher frequency energy (e.g., electron kinetic energy). Representative plots of one run are shown in Figs. (4 and 5). The exchange of electrostatic energy and ion kinetic energy is very clear, as is representative of ion plasma oscillations. When the plasma is made warm, lower hybrid oscillations are again observed. In addition, far better energy conservation was obtained (less than 1% error up to $\omega_{pe}t = 300$) for all ϵ tried from .6 to 1. At present we have not included spectral analysis on this code and therefore large (and strongly nonlinear) initial excitation was required to produce measurable oscillations.

The next step is twofold: first, to do extensive parameter studies and to understand the effects produced by those parameters, both physical and nonphysical; secondly, to add suitable diagnostics so that linear waves in warm plasmas may be studied. More physical simulation models could also be used, such as $\underline{k} \cdot \underline{B} \neq 0$.

REFERENCES

1. B. I. Cohen, T. A. Brengle, D. B. Conley, and R. P. Freis, "An Orbit-Averaged Particle Code", Lawrence Livermore Laboratory Report, UCRL-82832 (June 1979). Accepted for publication in J. Comp. Phys.

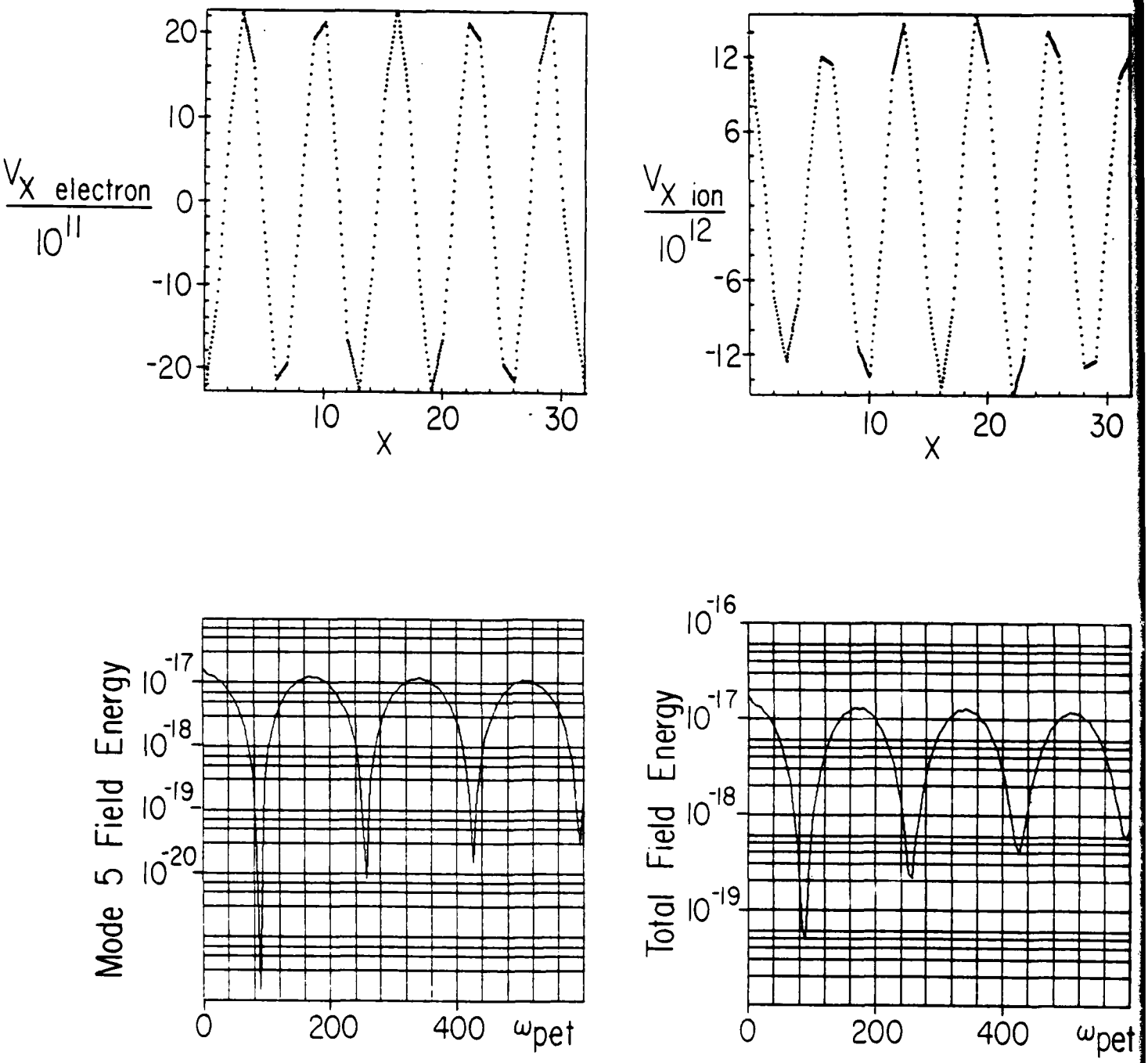

FIG. 4 Same parameters as in Fig. 3 except $\varepsilon = 2.0$. (a) electron phase space at $t = 299.985$ (b) ion phase space at $t = 298.5$ (c) mode 5 field energy from $t = 0$ to $t = 300$ (d) total field energy from $t = 0$ to $t = 300$.

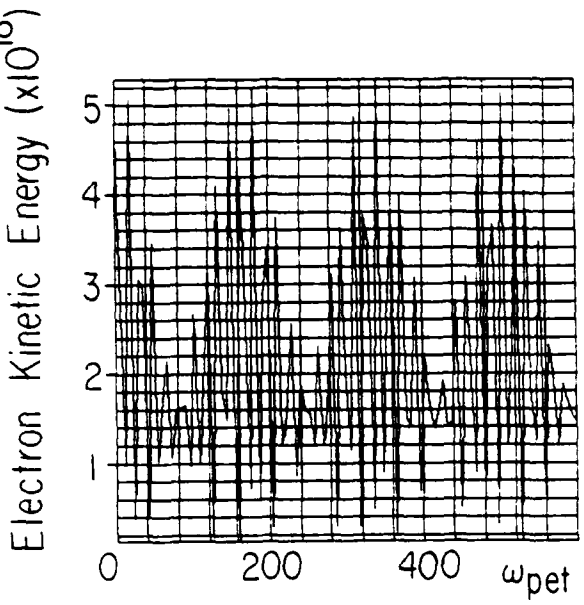

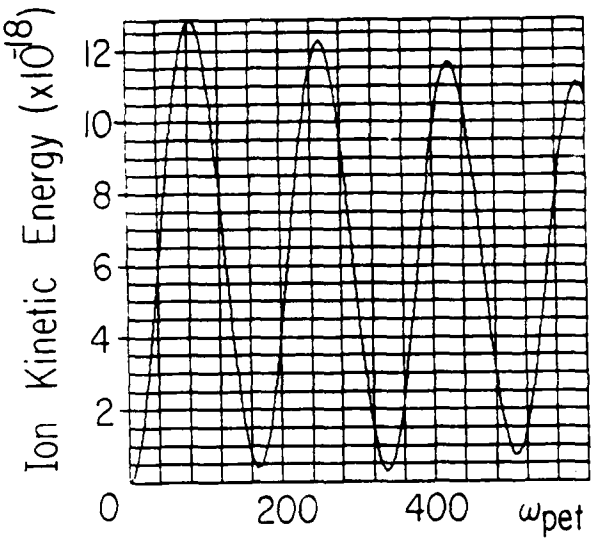

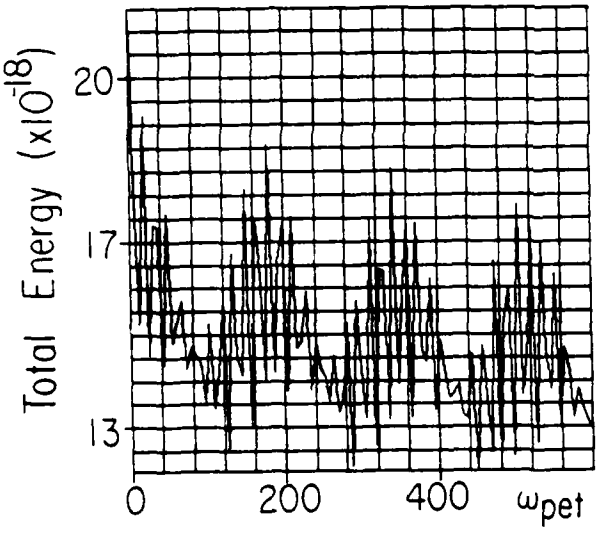

FIG. 5 Same parameters as in Fig. 4. (a) electron kinetic energy vs. time from t = 0 to t = 300 (b) ion kinetic energy from t = 0 to t = 300 (c) total energy from t = 0 to t = 300.

Section II

CODE DEVELOPMENT and MAINTENANCE

A. ES1 Code

See Orbit Averaging in Sec. I, Part E.

B. EM1 Code

No special progress to report.

C. EZOHAR Code

No special progress to report.

D. RINGHYBRID Code

This code is now being run with initialization provided by the RIGIDROTOR code as described in the section following, in the Sherwood abstract later in this QPR, and in an ERL report in preparation.

E. RIGIDROTOR Code (Field Reversed Equilibrium Solver)

Alex Friedman

The following is a copy of the LIBRIS abstract describing the RIGIDROTOR code; a brief description of the applications of this code appears elsewhere in this QPR.

---

77 Alex Friedman RIGIDROTOR

DATE- march, 1980 04/08/80 08:44:01

rigid rotor equilibrium solver and particle code initialization program

j. c. berkeley

electronics research laboratory, cory hall

university of california, berkeley ca 94618

415-642-3477

cdc 7600 fortran 1000 lines in use

ABSTRACT-

"rigidrotor" is a package which calculates field reversed equilibria using the time-independent vlasov equation, and outputs the fields and a set of particle initial conditions so that these equilibria may be used in particle simulations. the package was designed for use with the "ringhybrid" linearized 3d stability code, but is suitable for other axisymmetric particle or hybrid codes with minor modification.

in the present implementation, exponential rigid rotor vlasov equilibria, with distribution functions of the form f = c exp [- (h - omega * ptheta) / t], are computed on an r-z grid using an iteration scheme similar to that of sparks and finn.

the equation solved is :

$$l\, a = r\, dens\, thdot\, bnot \exp\left(\frac{psi - thdot\, bnot\, rsquared / 2}{psimax\ \ ctemp}\right)$$

where a = vector potential atheta, psi = r a, psimax = psi(o-point), l is the curlsquared operator, and the dimensionless variables are those used in the "ringhybrid" code, see cornell univ. lps rept. no. 268 (friedman, sudan, denavit). note that it is possible to arrange for the output to appear in any chosen units by setting bnot appropriately. the relation is atheta(outer wall) = bnot * nr / 2. thus, one need only figure out what atheta(outer wall) is in one's units, and then compute the correct bnot.

in these equilibria the current is carried entirely by hot ions with gyroradii which may range from infinitesimal (as in the hill vortex equilibria) to of order the system size (as in ion ring equilibria). a representation of the distribution function is obtained by assigning locations and velocities to particles in a manner which yields the correct density and mean azimuthal velocity in each grid cell, within small errors associated with finite particle size and the limited number of particles employed.

code usage and input variables are described on comment lines in the source itself.

REFERENCES-the first two references describe the program and the normalization, respectively, though the latter is not difficult to figure out from

the source, and the code is largely self-documented with comment lines. the latter references provide useful background information on field reversed equilibria.

---

a.friedman, proc.1980 sherwood meeting on theoretical aspects of controlled thermonuclear research (tucson, arizona).

a.friedman, r.n.sudan, and j.denavit, "a linearized 3d hybrid code for stability studies of field reversed ion rings," cornell university laboratory of plasma studies report no.268 (1979, submitted to j.comp.phys.)

l.sparks, j.m.finn, and r.n.sudan, bull.am.phys.soc.24, 955 (1979).

b.marder and h.weitzner, plasma phys.12, 435 (1970).

d.v.anderson, j.killeen, and m.e.rensink, phys.fluids 15, 351 (1972).

r.v.lovelace, d.a.larrabee, and h.h.fleischmann, phys.fluids 22, 701 (1979).

AVAILABILITY-

users can obtain a copy of the source from filem directory .takeme of user number 1234:

```
filem rds 1234 .takeme alwith. rr(esc)end / t v
```

the file thus obtained will be named rrmmddyy, where mm is the month, dd is the day, and yy is the year that the source was created. the source can be compiled using chatr; instructions appear on comment cards within the source. to list the source, type:

```
allout hsp <source> ccsp. seq. box <boxnumber> rigidrotor / t v
```

or

banner <usc> <source> ccsp. seq. box <boxnumber> rigidrotor / t v

where <usc> is the appropriate user service center designator, <source> is the name of the source file retrieved from filem, and <boxnumber> is the appropriate box number.

DISTRIBUTION- unlimited

F. Radial Code Notes (R,Rθ,RZ,RθZ)

C. K. Birdsall

Method C

Radial weighting may also be done to advantage with particles having charge density which is not uniform within the particle. Niels Otani has pointed out several advantages of using $\rho_{cloud} \sim 1/r$, such as: having the center of charge and mass at the arithmetic center; producing the familiar symmetric triangular particle shape when used with linear weighting independent of r; having a simple weighting algorithm (less operations than in Methods A and B). Let us see these in detail.

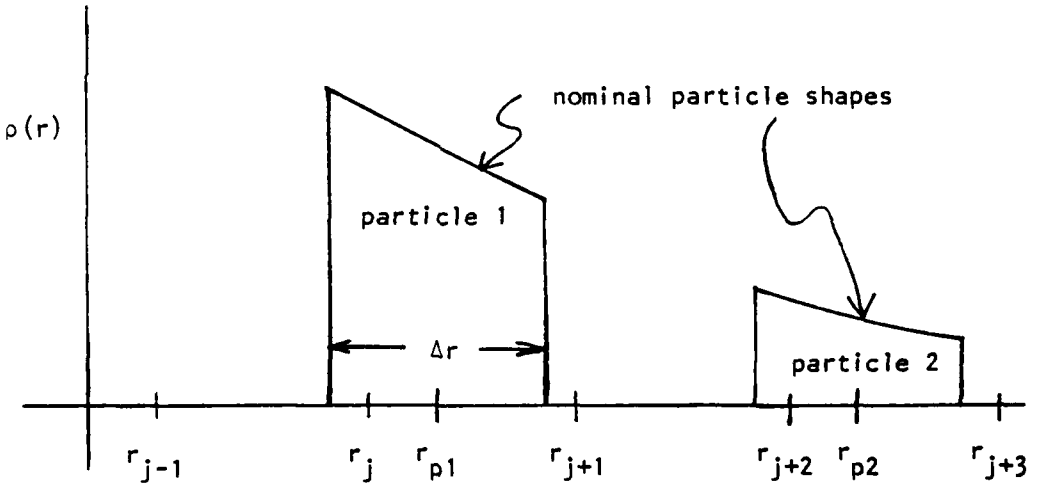

As the charge per unit radius is $\rho(r)2\pi rdrdz$ and $\rho(r) \sim 1/r$, this quantity is constant. Because charge/dr is flat (as it would be in an x-y grid), weighting charge to the grid r_j's can be done as in x-y grids. That is, the charge to be assigned to r_j of particles 1, by linear weighting, is

$$q(r_j) = q_p f$$

where f is the fraction of the nominal particle in the cell about r_j,

$$f = \int_{r_{p-\frac{1}{2}}}^{r_{j+\frac{1}{2}}} \rho_{\text{nominal}}(r)dV \Big/ \int_{r_{p-\frac{1}{2}}}^{r_{p+\frac{1}{2}}} \rho_n(r)dV$$

and $dV = rdrd\phi dz$. So, with $\rho_r \sim 1/r$

$$f = (r_{j+\frac{1}{2}} - r_{p-\frac{1}{2}})/(r_{j+\frac{1}{2}} - r_{j-\frac{1}{2}}) = a/\Delta r = (r_{j+1} - r_p)/\Delta r \ .$$

Similarly,

$$q(r_{j+1}) = q_p(b/\Delta r) = q_p(r_p - r_j)/\Delta r \ .$$

Note that there is no division by r_j of r_{j+1} or r_p as was true in Method A and B, simplifying the weighting. Note also that the particle shape as seen by the grid, that is, q(at r_j as r_p is varied) is simply the same as with linear weighting to rectangular grids. Thus, what is known about $S(\underline{x})$ particle shapes fits S(r). Also, the symmetric digital filtering used in rectangular grids, like (1,2,1) and compensation, like (-1,6,-1), may be used directly.

The θ weighting is simply linear interpolation, to be used as already given in Method B.

Hence, in 2d, full r,θ grid, Table 1 (of QPR IV, 1979) is simplified; the weights are

$$\left\{\frac{\text{weighted area}}{\text{total weighted area}}\right\} = \frac{[\delta r or(\Delta r - \delta r)]\alpha}{\Delta r \Delta \phi}$$

as in rectangular weighting. The charge weighting holds down to and at the origin, with no special consequences as $r_p \to 0$ or $r_p = 0$. The nominal particle density blows up as 1/r, but the total charge of the rod or ring does not.

B. I. Cohen notes that the charge density weighting of Method A, as used in SUPERLAYER etc., is proper for use with Poisson's equation, where charge density is wanted at the grid points, ρ_j and not q_j. (Finding charge at the grid points is more for use with Gauss' Law where charge inside some volume is accumulated.) Method A then uses linear weighting directly, weighting particle density to the grid. (The exercise given in the write-up of Method A on calculating the charge on the grid serves to check on charge conservation.)

QPR III 1979, p. 92 has $\rho_p = q_p/(\text{volume of charge})$ then gives $\rho_p = q_p/2\pi r_p \delta r \delta z$. This volume appears to be valid only in the limit $\delta r \to 0$. The exact volume is

$$\text{volume} = \int_{r_{inner}}^{r_{outer}} \iint r\,dr\,d\phi\,dz = \left(\frac{r_o^2 - r_i^2}{2}\right) 2\pi\delta z$$

$$= \left(\frac{r_o + r_i}{2}\right)(r_o - r_i)2\pi dz \ .$$

If the particle center is $r_p = (r_o + r_i)/2$ and particle thickness is $r_o - r_i = \delta r$, then the volumes are the same, with no need to consider $\delta r \to 0$.

G. POLARES: A Two-Dimensional Electrostatic R-θ Code

Niels F. Otani (Prof. C. K. Birdsall)

While it is often convenient and acceptable to approximate cylindrical systems with rectangular models, there are many cylindrical systems which exhibit effects not found in their rectangular counterparts. For example, the diocotron instability boundaries for a non-neutral hollow cylinder of charge depend explicitly on the inner and outer radius,[1] Clearly the nonlinear evolution of such a system would also be of some interest, and is easily studied using computer simulation.

With this in mind, we are in the process of developing a two-dimensional code which is based completely on the r-θ coordinate system (polar-electrostatic = POLARES), for use on the CRAY. An appropriate weighting scheme has been used to accumulate the charge density and fields on a radial grid, and, partly as an experiment, a grid of Fourier amplitudes has been used in the azimuthal direction. Both guiding-center and full-dynamics time-centered leapfrog movers have been incorporated in the program in such a way as to make them interchangeable for either species. A number of graphics packages have also been written. All are easily inserted into or removed from the main code or post-processor. Some allow interactive graphics viewing via DISSPLA. Further "modular" diagnostics packages are contemplated.

THE CODE

The program POLARES may be thought of as divided into five subunits: a main source (MAIN-S), a cliche file (INPCOMP), a binary module library (POLARLIB), the executable file (POLARES), and an input file (INPOLAR).

MAIN-S is a generally simple Fortran source usually consisting of common blocks and calls to various packages in POLARLIB. This format allows the user to insert various movers, charge weighting schemes, background charge distributions, diagnostics, graphics packages, etc., with ease, thus contributing to the flexibility of the code. One might suppose that this format results in a slow code; indeed, we find that the running speed is around 500,000 particle-time-steps per minute of computer time using a full-dynamics mover with 24 radial grid-points and 24 azimuthal Fourier modes. This is not particularly fast, but we have not made full use of the vectorization feature of the CRAY at the present time. Vectorization of the mover and charge accumulator should yield significant savings in time.

Common blocks and grid dimensions are loaded into MAIN-S and modules of the binary library POLARLIB during a precompiling sweep from information supplied by the cliche file INPCOMP. Thus the number of particles, grid points, and Fourier modes are easy to change.

POLARLIB contains all the main building blocks of the simulation. These include graphics packages compatible with POLARES, diagnostics, grid charge accumulators, movers, initializing routines, a particle loader, and a field solver. Further development, refinement, and testing of most of these routines is envisioned; additional diagnositcs and graphics packages are also expected to be created.

Some of the more important routines are outlined here.

RHOEWT and RHOIWT accumulate charge density on the grid from particle electrons and ions respectively. One may envision the charge weighting scheme as follows. We first lay on the polar plane a series of concentric circles each Δr outside the one before it, out to a maximum radius a. These represent the grid points, probably more properly called grid circles.

Each charged particle with coordinates (r_i,θ_i) is separated into two charged particles of charge $(r_{j+1}-r_i/\Delta r)q$ and $(r_i-r_j/\Delta r)q$ located at (r_j,θ_i) and (r_{j+1},θ_i), respectively. Here r_j and r_{j+1} are the radii of the two nearest grid circles, and q is the charge (per unit length). (By charge particles in this code we of course refer to line charges extending infintely in both directions parallel to the cylindrical axis of symmetry.) Each fractional line charge is now considered as a sum of sinusoidal waves existing only on its own grid circle according to the formula

$$\rho(\theta) = \frac{q'}{2\pi r'}\left(1 + 2\sum_{m=1}^{M}(\cos m\theta_i \cos m\theta + \sin m\theta_i \sin m\theta)\right)$$

where q' is the fractional charge of the sub-particle located on the grid circle of radius r'. The weighting factor 1/r' arises from the formula for a delta function in polar coordinates:

$$\delta^2(\underset{\sim}{x}-\underset{\sim}{x}_i) = \frac{1}{2\pi r_i}\delta(r-r_i)(1+2\sum_{m=1}^{\infty}\cos m(\theta-\theta_i)) \ .$$

The θ shape function will be made more general, essentially just changing the coefficients in the sum, e.g., to drop off as $1/m^2$, implying a broader particle, say, $\Delta\theta$ wide, where $\Delta\theta$ is something like $2\pi/M$. Thus Fourier amplitudes of the charge density are accumulated for each of the mode numbers up to M for each of the $a/\Delta r$ grid circles. Notice that we cannot have a grid circle of radius zero in the scheme. Therefore, in order to deal with particles inside the first grid circle, we have devised a somewhat ad hoc scheme. The idea is to replace each eligible particle with an equivalent charge distribution on the first grid circle. By "equivalent" we

mean that the new charge distribution produces the same potential outside the first grid circle as did the charge it replaces. Thus for particles with $r_i < \Delta r$ we use the Fourier amplitudes implied by the charge distribution

$$\rho(\theta) = \frac{q}{2\pi\Delta r}\left(1 + 2\sum_{m=1}^{M}\left(\frac{r_i}{r}\right)^m (\cos m\theta_i \cos m\theta + \sin m\theta_i \sin m\theta)\right) .$$

This scheme has the advantages that (a), the long range force is correct and (b), a particle crossing the first grid circle is represented by continuously varying charge density quantities. Figure (1a) illustrates the charge density resulting from a single point charge.

Once a charge density has been established on the grid, the next step is to solve for the potential and electric fields. This is accomplished by the subroutine GRFIELDS. The task of GRFIELDS is fairly straightforward; a tridiagonal solver is used to find the Fourier components of the potential Φ_{jm} from the finite difference version of the Poisson equation

$$\frac{1}{r}\frac{\partial}{\partial r} r \frac{\partial \Phi_m}{\partial r} - \frac{m^2}{r^2}\Phi_m = -4\pi\rho_m$$

namely,

$$\frac{\Phi_{(j+1)m} - 2\Phi_{jm} + \Phi_{(j-1)m}}{(\Delta r)^2} + \frac{1}{r_j}\frac{\Phi_{(j+1)m} - \Phi_{(j-1)m}}{2\Delta r} - \frac{m^2}{r_j^2}\Phi_{jm} = -4\pi\rho_{jm} .$$

The potential is then used to find the electric fields:

$$(E_r)_{jm} = \frac{\Phi_{(j-1)m} - \Phi_{(j+1)m}}{2\Delta r}$$

$$(E_\theta)^{(\frac{c}{s})}_{jm} = -\frac{m}{r_j}\Phi^{(\frac{s}{c})}_{jm} .$$

In the last formula, the c/s notation is meant to indicate that the cos mθ coefficients of $(E_\theta)_{jm}$ are derived from sin mθ coefficients of Φ_{jm}, and similarly the sin mθ coefficients are derived from the cos mθ coefficients, with a change of sign. The multiplication by m (for $\nabla\phi$ angular component) may be replaced by something like mdif(mΔθ) to imply a more local gradient; also, both components might be weighted to reduce angle errors in $\underline{E}$; these techniques are common to xy codes.

At present the boundary conditions imposed are (a) $\Phi_{jm} = 0$ at $r = a$ for all m and (2) $\Phi_{jm} = 0$ at $r = 0$ for all $m \neq 0$ and $\Phi_{0m} = \Phi_{1m}$ for $m = 0$. This corresponds to a system surrounded by a conducting cylindrical wall of radius a.

The electric fields and potential are illustrated in Figure 1. Notice the ripple in E_r and E_θ at the radius of the point charge. This is due to the ripple in the charge density. It is anticipated that smoothing in the Fourier space of θ, or using a line charge broadened into a finite size rod will eliminate this undesirable effect.

The particles are advanced to their new positions by one of the movers available from POLARLIB. Thus far electron and ion guiding-center movers MOVEGC and MOVIGC and ion full-dynamics mover MOVIES have been written. All movers find the electric fields at each particle by reversing the steps RHOIWT and RHOEWT used to compute the charge density. That is, for a particle located at (r_i,θ_i), the electric fields are first found at (r_j,θ_i) and (r_{j+1},θ_i) by (for δ function weighting in θ)

$$\underset{\sim}{E}(r_j,\theta_i) = \frac{1}{2\pi}\left(\underset{\sim}{E}_{oj} + 2\sum_{m=1}^{M}\left(\underset{\sim}{E}_{mj}^{(c)}\cos m\theta + \underset{\sim}{E}_{mj}^{(s)}\sin m\theta\right)\right)$$

and then are interpolated to the particle by linear weighting

$$\underset{\sim}{E}(r_i,\theta_i) = \underset{\sim}{E}(r_j,\theta_i)\left(\frac{r_{j+1}-r_i}{\Delta r}\right) + \underset{\sim}{E}(r_{j+1},\theta_i)\left(\frac{r_i-r_j}{\Delta r}\right) .$$

The guiding-center mover uses this value of $\underset{\sim}{E}$ to compute a guiding-center velocity from the equation

$$\underset{\sim}{v}_{new} = c_1\,\underset{\sim}{E}\times\underset{\sim}{B} + c_2\,\underset{\sim}{g}\times\underset{\sim}{B}$$

where c_1 and c_2 are appropriate constants.

The full-dynamics mover obtains the new velocities from the old velocities using a method analogous to the one employed in A. B. Langdon's one-dimensional electrostatic code ES1:

$$(v_r)_1 = (v_r)_{t-\frac{1}{2}\Delta t} + \frac{q}{m}(E_r)_t\frac{\Delta t}{2}$$

$$(v_\theta)_1 = (v_\theta)_{t-\frac{1}{2}\Delta t} + \frac{q}{m}(E_\theta)_t\frac{\Delta t}{2}$$

$$(v_r)_2 = (v_r)_1\cos\omega_c\Delta t + (v_\theta)_1\sin\omega_c\Delta t$$

$$(v_\theta)_2 = -(v_r)_1\sin\omega_c\Delta t + (v_\theta)_1\cos\omega_c\Delta t$$

$$(v_r)_{t+\frac{1}{2}\Delta t} = (v_r)_2 + \frac{q}{m}(E_r)_t\frac{\Delta t}{2}$$

$$(v_\theta)_{t+\frac{1}{2}\Delta t} = (v_\theta)_2 + \frac{q}{m}(E_\theta)_t\frac{\Delta t}{2}$$

where $\omega_c \equiv qB_o/mc$.

Both movers then move particles to their new positions according to

$$r_{t+\Delta t} = \sqrt{(r_t+(v_r)_{new}\Delta t)^2 + (v_\theta)^2_{new}\Delta t^2}$$

$$\approx r_t + (v_r)_{new}\Delta t + \frac{1}{2}\frac{(v_\theta)^2_{new}\Delta t^2}{r_t}$$

$$\theta_{t+\Delta t} = \theta_t + \arctan\frac{(v_\theta)_{new}\Delta t}{r_t+(v_r)_{new}\Delta t}$$

$$\approx \frac{(v_\theta)_{new}\Delta t}{r_t}\left(1 + \frac{(v_r)_{new}\Delta t}{r_t}\right)$$

where $\underline{v}_{new} \equiv \underline{v}_{t+\Delta t/2}$ for the full-dynamics mover.

The approximations given are valid for $v\Delta t/r \ll 1$. At present we use the approximate formulas for particles with $r_t > \Delta r$ and $r_{t+\Delta t} > \Delta r$. If the approximate formula yields $r_{t+\Delta t} < \Delta r$ or if $r_t < \Delta r$, the exact formulas are used.

Finally the new velocities of both guiding-center and full-dynamics movers must be expressed in the new local coordinate system:

$$v_r \rightarrow v_r \cos\Delta\theta + v_\theta \sin\Delta\theta$$

$$v_\theta \rightarrow -v_r \sin\Delta\theta + v_\theta \cos\Delta\theta$$

where $\Delta\theta = \theta_{t+\Delta t} - \theta_t$. Again, away from the origin we use

$$\cos\Delta\theta \approx 1 - \frac{(\Delta\theta)^2}{2}, \quad \sin\Delta\theta \approx \Delta\theta .$$

The offset of the velocities from the positions in the full-dynamics mover is necessary for the mover to be time-centered. The offset is accomplished at the beginning of the run by the routine SETIV for ions (and SETEV for electrons, to be written), by

$$(v_r)_1 = v_{ro} - \frac{q}{m} E_{r0} \frac{\Delta t}{2}$$

$$(v_\theta)_1 = v_{\theta o} - \frac{q}{m} E_{\theta 0} \frac{\Delta t}{2}$$

$$(v_r)_{-\Delta t/2} = (v_r)_1 \cos \frac{\omega_c \Delta t}{2} - (v_\theta)_1 \sin \frac{\omega_c \Delta t}{2}$$

$$(v_\theta)_{-\Delta t/2} = (v_r)_1 \sin \frac{\omega_c \Delta t}{2} + (v_\theta)_1 \cos \frac{\omega_c \Delta t}{2} \quad .$$

Initial particle positions and velocities are read into the code from an input file (INPOLAR) by the POLARLIB module LOADR.

PRELIMINARY RESULTS

The code has been tried on a few systems, the time evolutions of which are known.

Figure (2) shows one particle moving in the field of another fixed particle. There is also a uniform external magnetic field present. The charge does not feel the effects of its own wall image. We expect the $\underline{E} \times \underline{B}$ motion of the particle to be along an equipotential and to be fastest where $|\underline{E}|$ is largest. The computed trajectories are consistent with these expectations. Notice the effect of the ripple of the fixed charge, especially evident when the guiding-center mover is used.

Figure (3) shows some snapshots of an instability in a ring of charge in a uniform magnetic field, simulated using the guiding-center mover. Theory for the diocotron instability predicts all modes below m = 6 should be unstable for our parameters.[1] This seems to be consistent with our simulation.

Figure (4) illustrates the charged-sheet instability which has been observed in electron beams and is believed to occur in auroral displays.[2] The mover used here is the full-dynamics mover, but the guiding-center mover produced qualitatively very similar results. This allows us to be somewhat confident that both movers are working correctly.

Figure (5) illustrates our attempt to simulate the Rayleigh-Taylor instability of a neutral plasma moving in a gravitational field directed radially outward. g simulates either ∇B or R drifts, which are signed, hence lead to flute instabilities. The ions are pushed with a full-dynamics mover while a guiding-center mover is used for the electrons. We observe some peculiar behavior in the vicinity of the origin. This is quite likely an artifact of the code and will be investigated in the near future. As is obvious in the figure, the growth of the instability is quite rapid. When gravity of the same magnitude is directed inward, the plasma is found to be stable. We also find a mild growth rate even in the absence of gravity. This is possibly due to expansion of the warm plasma (in uniform B) or the abnormally large field fluctuations likely to be associated with so few particles (1024 ions, 1024 electrons). The large time step used in this preliminary run ($\omega_c \Delta t = 1$) is also a possible cause.

Finally, plasma oscillations have been observed in a cylindrical plasma. In this run, the electrons were pushed using the full-dynamics mover with no external magnetic field present, and the ions were fixed. The frequency of oscillation was not correct however;

we found oscillations occurring at about ω_{pe}, instead of the theoretical value of $\omega_{pe}/\sqrt{2}$, the dipole resonance frequency. (Actually, in the presence of the wall, and with our parameters, the theoretical resonant frequency is lowered slightly to $2\omega_{pe}/3$.) No explanation for the discrepancy is offered at this time.

FUTURE DEVELOPMENTS

The code POLARES has thus far produced encouraging results though most are as yet qualitative in nature. It is hoped that further work with the code will produce quantitative results and clear up problems already encountered.

Definitely on the agenda are vectorization, which should result in considerable savings in computer time, smoothing in θ-Fourier space, and improvement in the diagnostics. Results of these developments will be reported in a future QPR.

REFERENCES

1. Janes, G. S. et al., "New Type of Accelerator for Heavy Ions", Physical Review 145, May, 1966, pp. 925-952.
2. Webster, Harold F., and Hallinan, Thomas J., "Instabilities in Charge Sheets and Current Sheets and Their Possible Occurrence in the Aurora", Radio Science 8, May, 1973, pp. 475-482.

FIGURE CAPTIONS

FIG. 1. Charge density, potential, and electric fields (in arbitrary units) generated by a line charge located at $r = 16\Delta r$, $\theta = \pi/2$. The radial grid appearing in the plots is real, but the θ-grid is generated by the plotting routine. $a = 24\Delta r$, $M = 24$.

FIG. 2. Orbit of a positively-charged particle in the field of a fixed positively-charged particle located at $r = 16\Delta r$, $\theta = \pi/2$. $a = 24\Delta r$, $M = 24$.

(a) Full-dynamics mover: in cgs, $4\pi q^2 \Delta t^2/m = 2$, $qB_o \Delta t/mc = 0.5$, 1500 timesteps. Initial conditions for the mobile particle: $r = 8\Delta r$, $\theta = \pi/2$, $v_r \Delta t = 0$, $v_\theta \Delta t = 0.667$.

(b) Guiding-center mover: in cgs, $4\pi qc\Delta t/B_o = 2$, 3000 timesteps. Initial conditions: $r = 6.667\Delta r$, $\theta = \pi/2$.

FIG. 3. Instability in a charged ring using the guiding-center mover, 1024 particles uniformly distributed between $r = 9\Delta r$ and $r = 11\Delta r$, $4\pi qc\Delta t/B_o = 0.02$, $a = 16\Delta r$, $M = 16$.

FIG. 4. Charged-sheet instability using the full-dynamics mover with 1024 particles, $\omega_p \Delta t = 0.9$, $\omega_c \Delta t = 1$, $a = 24\Delta r$, $M = 24$.

FIG. 5. Simulation of a uniformly-magnetized plasma in a gravitational field directed radially outward. A full dynamics ion mover and an $\underset{\sim}{E} \times \underset{\sim}{B}$ guiding-center electron mover are used. Initially the plasma is uniformly distributed at radius $8\Delta r$. Parameters: $\omega_{ci} \Delta t = 1$, $\omega_{pi} \Delta t \cong 0.22$, $\omega_{pe}^2/|\omega_{ce}| = \omega_{pi}^2/\omega_{ci}$, $g = 0.0625(r/\Delta r)$ grid points$/(\Delta t)^2$, 1024 electrons, 1024 ions, $a = 24\Delta r$, $M = 24$.

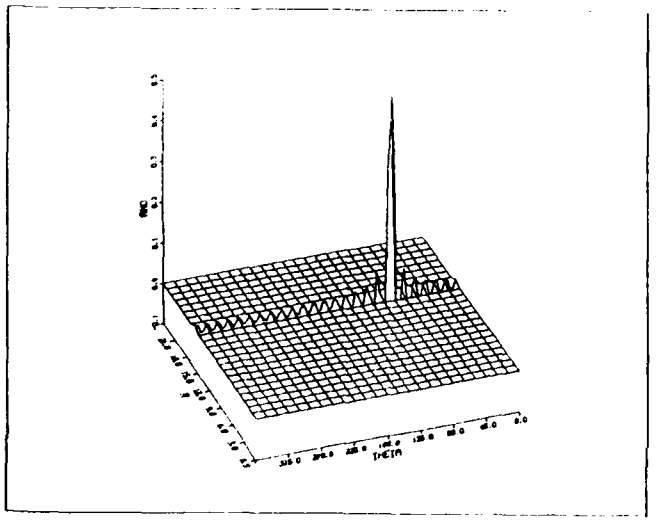

(a) CHARGE DENSITY

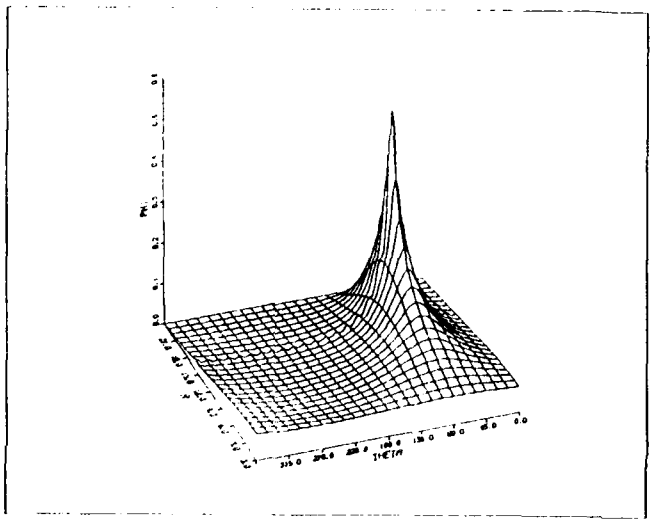

(b) POTENTIAL

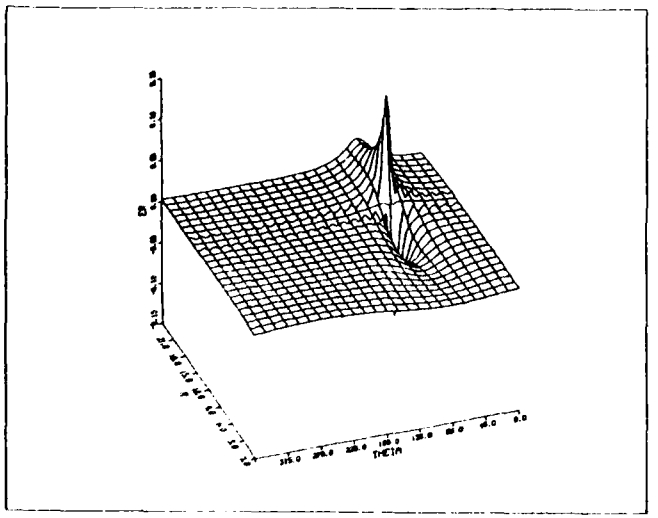

(c) E_r

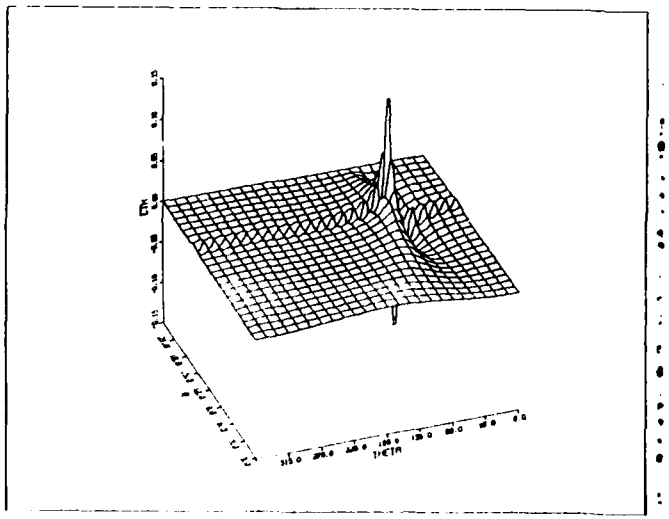

(d) E_θ

FIGURE 1

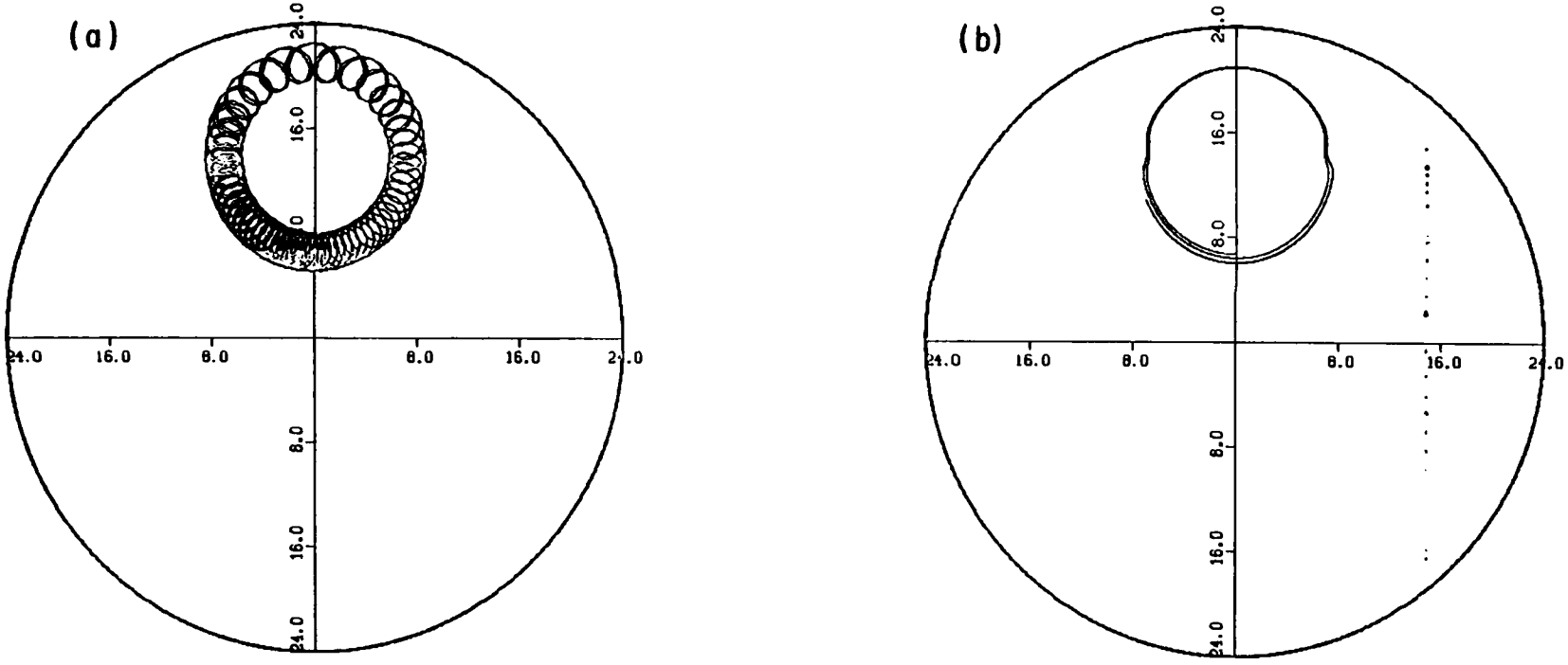

FIGURE 2

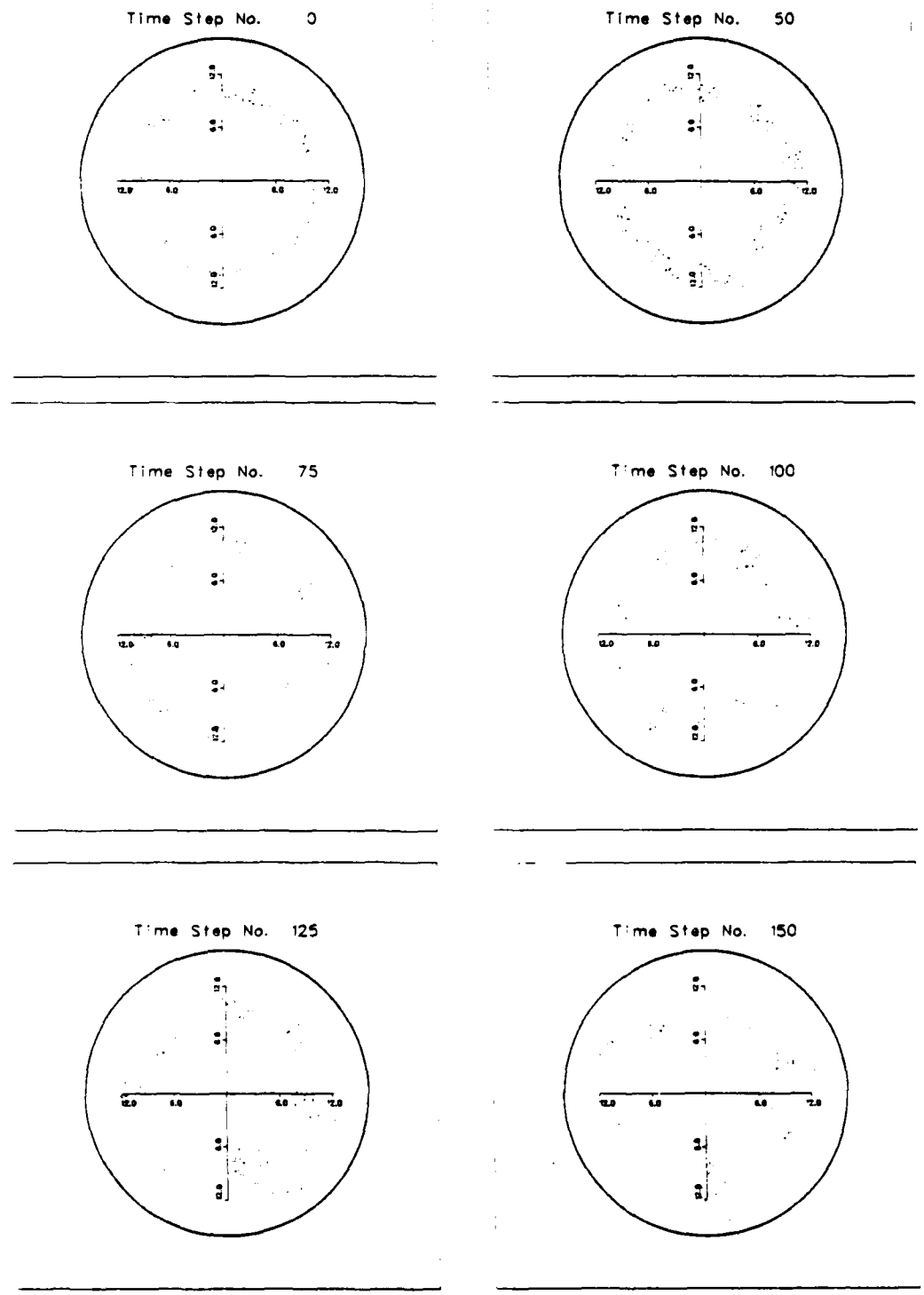
Time Step No. 0
Time Step No. 50
Time Step No. 75
Time Step No. 100
Time Step No. 125
Time Step No. 150

FIGURE 3

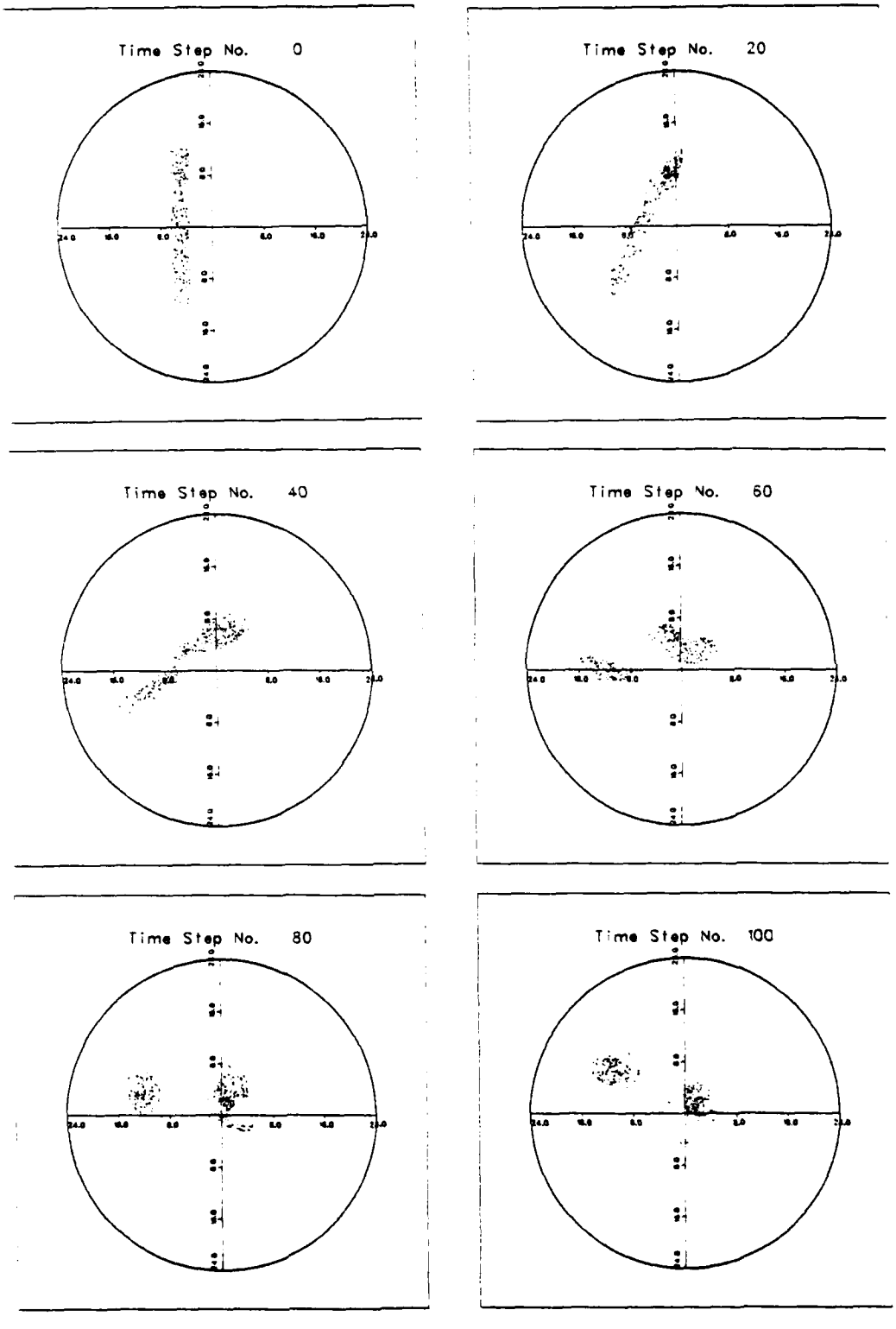
Time Step No. 0
Time Step No. 20
Time Step No. 40
Time Step No. 60
Time Step No. 80
Time Step No. 100

FIGURE 4

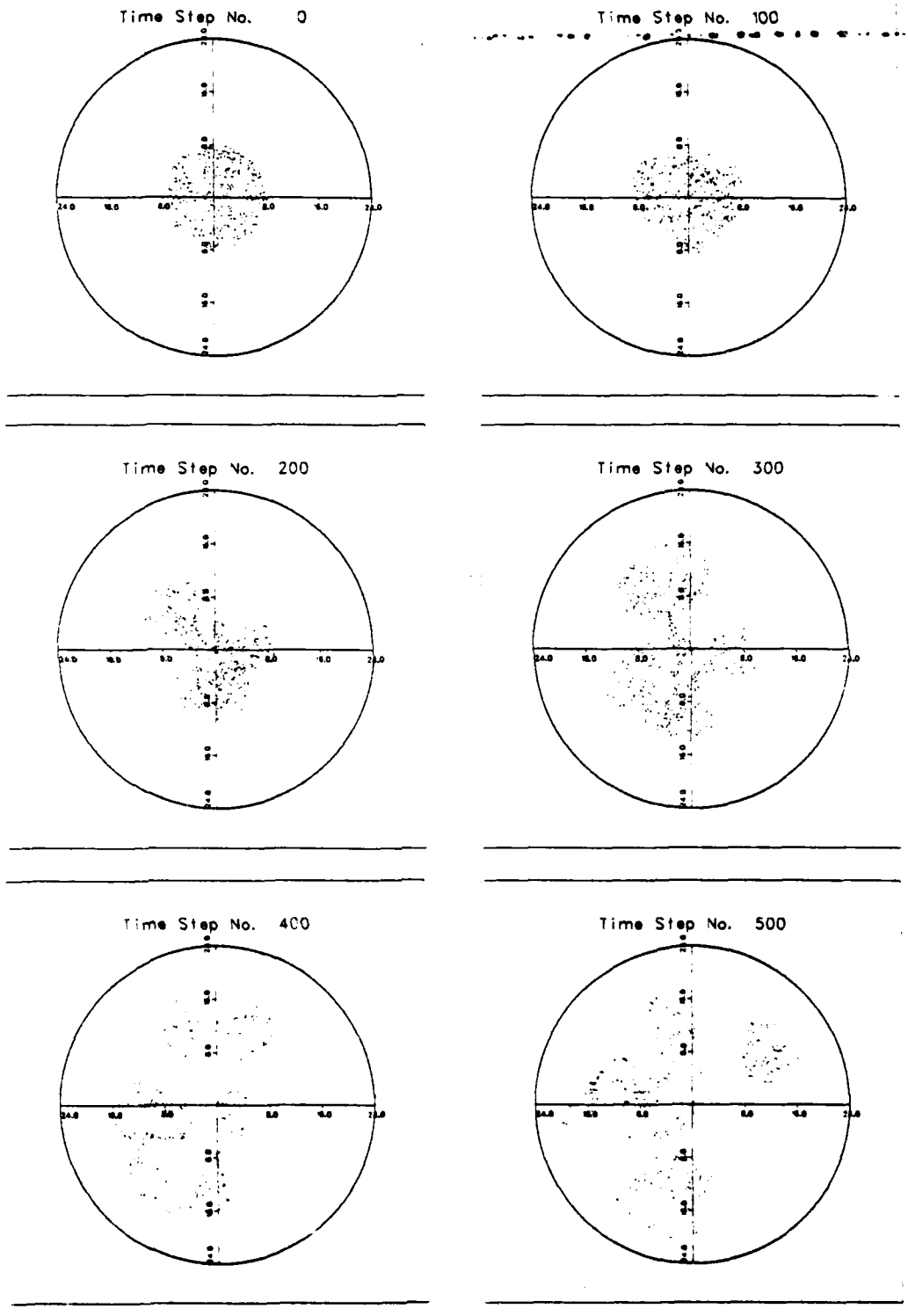
Time Step No. 0
Time Step No. 100
Time Step No. 200
Time Step No. 300
Time Step No. 400
Time Step No. 500

FIGURE 5

H. Dispersion Relation Solver for a Linearized Two-Fluid Uniform Plasma Model

Niels F. Otani (Prof. C. K. Birdsall)

A simple solver is being developed for the dispersion relation associated with a linearized, magnetized, electromagnetic, two-fluid, uniform plasma model. The model allows an isotropic temperature for each species. The unperturbed quantities n_o, T_s, and B_o are uniform in space and constant in time, and neither species is allowed to drift. The linearized equations required to describe this system are then as follows:

$$\frac{\partial}{\partial t}\delta n_s + n_o \nabla \cdot \delta \underline{v}_s = 0$$

$$\frac{\partial \underline{v}_s}{\partial t} = -\frac{\gamma_s T_s}{m_s}\nabla\frac{\delta n_s}{n_o} + \frac{q_s}{m_s}\left(\delta\underline{E} + \frac{\delta \underline{v}_s}{c}\times\underline{B}_o\right)$$

$$\nabla\times\delta\underline{B} = \frac{4\pi n_o}{c}\sum_s q_s \delta\underline{v}_s + \frac{1}{c}\frac{\partial\delta\underline{E}}{\partial t}$$

$$\nabla\times\delta\underline{E} = -\frac{1}{c}\frac{\partial\delta\underline{B}}{\partial t}$$

where s refers to the species involved (here electrons and ions). This code is intended as an educational aid only; the zoo of small-amplitude waves and oscillations resulting from this set of equations has been well-understood for some time.

Allowing the perturbed quantities to have the dependence $\exp(i(k\cdot r - \omega t))$, the dispersion relation for this set of equations is easily found to be[1]

$$\det\left[\underset{\sim}{\beta}(\omega,\underset{\sim}{k}) + \sum_s \omega_s^2 \underset{\sim}{\alpha}(\omega,\underset{\sim}{k})\right] = 0$$

$$\underset{\sim}{\alpha}_s \equiv \frac{1}{1 - a_s - b_s^2(1 - a_s\cos^2\theta)} \cdot$$

$$\begin{bmatrix} 1 - a_s\sin^2\theta - b_s^2 & a_s\sin\theta\cos\theta & ia_sb_s\sin\theta\cos\theta \\ a_s\sin\theta\cos\theta & 1 - a_s\cos^2\theta & ib_s(1 - a_s\cos^2\theta) \\ -ia_sb_s\sin\theta\cos\theta & -ib_s(1 - a_s\cos^2\theta) & 1 - a_s \end{bmatrix}$$

$$\underset{\sim}{\beta}_s \equiv \begin{bmatrix} k^2c^2\sin^2\theta - \omega^2 & -k^2c^2\sin\theta\cos\theta & 0 \\ -k^2c^2\sin\theta\cos\theta & k^2c^2\cos^2\theta - \omega^2 & 0 \\ 0 & 0 & -\omega^2 \end{bmatrix}$$

$$a_s \equiv \frac{\gamma_s KT_s}{m_s}\frac{k^2}{\omega^2} \qquad b_s \equiv \frac{\Omega_s}{\omega}$$

$$\cos\theta = \frac{\underset{\sim}{B}_o \cdot \underset{\sim}{k}}{|\underset{\sim}{B}_o||\underset{\sim}{k}|}$$

$$\Omega_s \equiv \frac{q_s B_o}{m_s c}$$

$$\omega_s^2 \equiv \frac{4\pi n_o q_s^2}{m_s} \cdot$$

The dispersion relation may be expressed as a 30th-degree polynomial in ω, but generally most of the roots are zero. The code therefore samples the value of the polynomial at ω_{test} amd $2\omega_{test}$ where ω_{test} is much

smaller than any frequency intrinsic to the free parameters of the system. Then $\log_2 f(2\omega_{test})/f(\omega_{test})$ factors of ω are divided out of the polynomial f, and the new function is used in Steven Au-Yeung and Alex Friedman's root solver code SOLVER[2] to obtain the various branches of $\omega(|\underset{\sim}{k}|)$ (θ fixed). This procedure is necessary as SOLVER often has trouble with functions having several equal roots. An example of the output is shown in Fig. 1.

Future development of the code will allow plotting of $\omega(\theta)$ ($|k|$ fixed) and also permit the user to obtain relative amplitudes and phases of $\delta\underset{\sim}{E}$, $\delta\underset{\sim}{B}$, δn, $\delta\underset{\sim}{v}$, etc., which provide information about the nature of the mode. Either the subroutines used with SOLVER or a complete code will be made available to users.

REFERENCES

1. Allis, W. P., Buchsbaum, S. J., and Bers, A., Waves in Anisotropic Plasmas. Ch. 1. M.I.T. Press, 1963.

2. Au-Yeung, H. Stephen, and Friedman, Alex. "SOLVER: An Analytic Function Root Solving and Plotting Package." Electronics Research Laboratory: University of California, Berkeley, August, 1979. Memorandum No. UCB/ERL M79/55.

I. RJET Development

No special report.

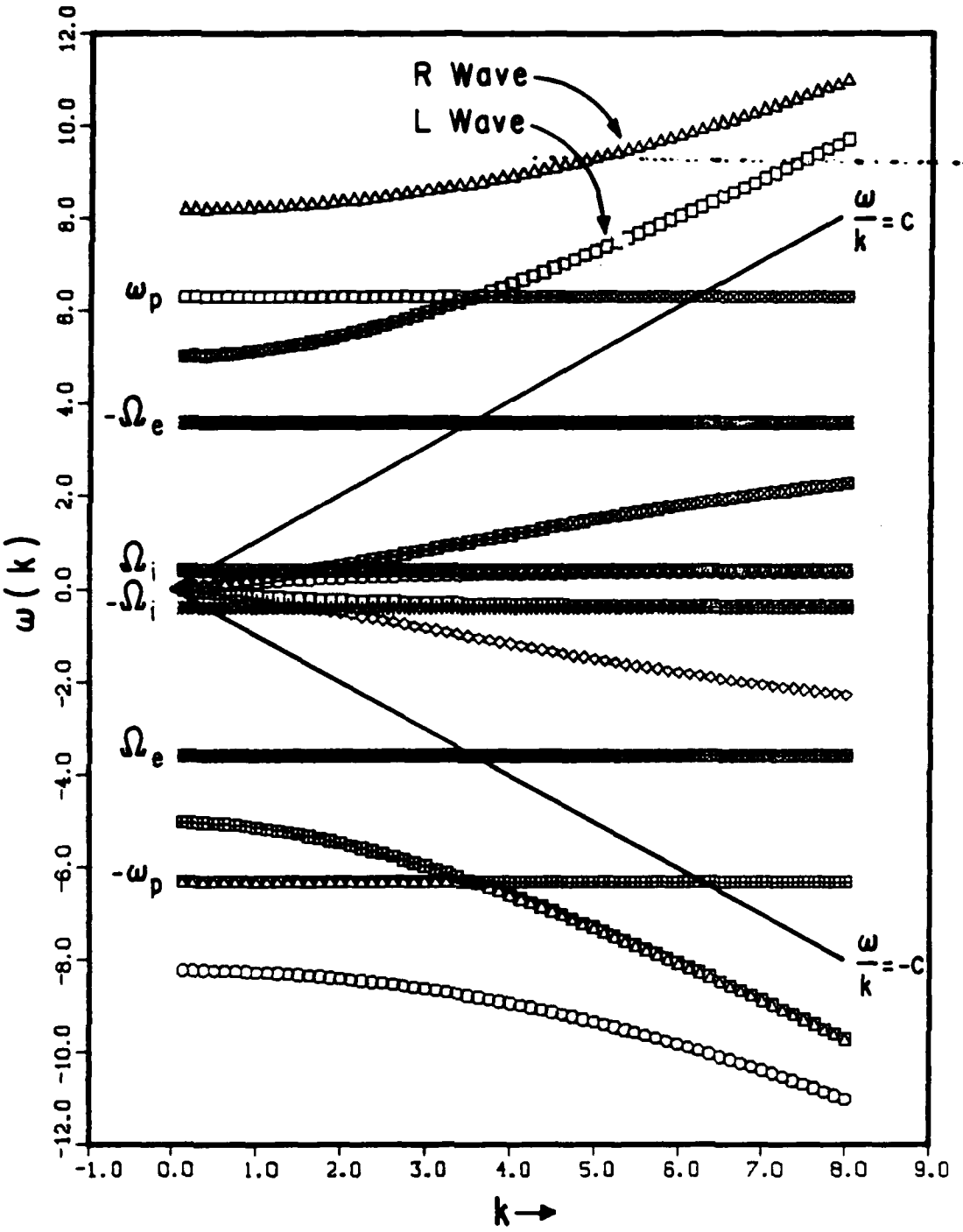

FIG. 1 Program output generated for c=1, θ=0 ($k_\perp$=0), Ω_e=-3.6, Ω_i=0.4, ω_{pe}=6, ω_{pi}=2 with labels and velocity-of-light lines added. Notice how the electron- and ion-cyclotron modes merge into the Alfven mode at low k. Also present are the R- and L-electromagnetic modes as well as bands marking the characteristic frequencies Ω_e, Ω_i, and $\omega_p=\sqrt{\omega_{pe}^2+\omega_{pi}^2}\approx 6.32$.

J. Software Developments

Niels F. Otani

A utility routine, DD80MAKE, has been created for use on the A-machine for the purpose of facilitating the conversion of fr80 files into dd80 files. The code is especially useful when several fr80 files have been generated on the A-machine or sent from the Cray to be viewed as dd80 files using TEKPLOT. The routine may be obtained from FILEM by typing:

filem rds 1210 .public dd80make

DD80MAKE is a LIB-created library and contains the executable file as the first entry. Also included in the library are the source and the utility routine DDEX. The latter is a dd80 file editor described in a previous GPR[1] which is often useful in conjunction with this program.

The execute line for DD80MAKE is:

dd80make box bnn anyid [end] / t v

If the box and id are omitted, DD80MAKE will prompt for this information.

If "end" is omitted in the execute line, dd80make will attempt to convert any files beginning with "f105" into dd80 files. The new dd80 files will retain the two identifying characters of their old fr80

counterparts, but however will begin with "dx". The old fr80 files are then deleted from the file index. The program subsequently goes to sleep for approximately one minute, then wakes up, again examines the file index for any new files beginning with "f105", and if so converts them into dd80 files. This process goes on indefinitely until "control-e i" is typed at which time the program terminates.

If "end" is entered as the last word on the execute line, the code will examine the user's files only once for files beginning with "f105", convert the ones it finds into dd80 files, and terminate.

One word of caution--the routine uses a non-insignificant amount of computer time in the suspended mode of operation (approximately 0.02 minutes/hour at priority 1); therefore it is advisable to not run the code at a low priority in this mode. It is anticipated that this difficulty will be corrected shortly.

Ap-Kaung, Stephen, and Friedman, Alex. "First Quarter Progress Report on Plasma Theory and Simulation." U. of California, Berkeley: 1979. p33.

Section III

PLASMA SIMULATION TEXT

A contract has been signed with McGraw-Hill for the text to be delivered to them Dec. 1, 1980, duly shortened and updated. No further progress will be reported here.

Section IV

SUMMARY of REPORTS, TALKS, PUBLICATIONS

Abstracts of papers to be presented at the Sherwood Fusion Theory Meeting April 23-25 at the University of Arizona, Tucson follow.

A listing of papers dealing with instabilities due to currents in diode regions is also given.

FRM and ION RING EQUILIBRIA for the RINGHYBRID CODE*

Alex Friedman
Electronics Research Laboratory
University of California
Berkeley, CA 94720

We have developed a new method of generating axisymmetric field reversed equilibria for the RINGHYBRID code, a linearized 3d hybrid code used for studies of the low-frequency stability of such configurations[1,2]. Equilibria of known functional form are calculated numerically, and appropriate particle initial condition and magnetic field data are used to initialize the hybrid code.

Exponential rigid rotor Vlasov equilibria, with distribution functions of the form $f \propto \exp[-(H-\Omega P_\theta)/T]$, are computed on an r-z grid using an iteration scheme similar to that of Sparks and Finn[3]. In these equilibria the current is carried entirely by hot ions with gyroradii which may range from infinitesimal (as in the Hill vortex equilibria) to the order of the system size (as in ion ring equilibria). A representation of the distribution function is obtained by assigning locations and velocities to particles in a manner which yields the correct density and mean azimuthal velocity in each grid cell, within small errors associated with finite particle size and the limited number of particles employed (several thousand). RINGHYBRID advances these particles along their equilibrium orbits in the time-independent, self-consistent zero order field. (For stability studies the code simultaneously advances linearized displacements from these orbits, as well as linearized quasineutral fluid equations for cold ion and electron components, and self-consistent first order E and B fields, which are fully 3d.)

A variety of field reversed mirror and ion ring equilibria have been obtained; when the equilibrium field and particle initial condition data are used in RINGHYBRID, particle moments remain nearly constant in time. Orbits are, in general, quite complicated, and preliminary indications are that many are truly stochastic[2]. The complexity of moderate-gyroradius FRM orbits arises from the fact that particles moving along closed field lines may or may not reflect in the high field regions, and furthermore may pass near the field null during their gyratory excursions. Also, the rate of a particle's azimuthal drifting motion depends strongly upon where it lies on its orbit in the r-z plane.

Previously, equilibria were generated by injecting bursts of particles into an external magnetic field and solving Ampere's law (with a resistive source term $-\sigma_o \partial A_\theta/\partial t$ included to damp collective oscillations) repeatedly until A_θ became nearly stationary. While this produced equilibria which were useful for ion ring stability studies[2], the new method affords greater control over the resulting equilibria, and so parameters may more readily be varied.

The package which computes equilibrium fields and particle initial conditions is called RIGIDROTOR, and is available for general use through LIBRIS on the NMFECC CDC-7600.

*Research supported by the U.S. Department of Energy under Contract No. DE-AS03-76SF00034, Project Agreement No. DE-AT03-76ET53064.

[1]A. Friedman, R. N. Sudan, and J. Denavit, Proc. Eighth Conf. on Numerical Simulation of Plasmas, Paper No. PC-13, Lawrence Livermore Lab. Conf. Proc. No. CONF-780614 (1978); Cornell Univ. Lab. of Plasma Studies Rept. No. 268 (1979, to appear in J. Comp. Phys.).
[2]A. Friedman, J. Denavit, and R. N. Sudan, Bull. Am. Phys. Soc. 24, 956 (1979).
[3]L. Sparks, J. M. Finn, and R. N. Sudan, Bull. Am. Phys. Soc. 24, 955 (1979).

SATURATION OF THE LOWER-HYBRID DRIFT INSTABILITY*

Yu-Jiuan Chen & C. K. Birdsall
Electronics Research Laboratory
University of California
Berkeley, CA 94720

Bruce I. Cohen
Lawrence Livermore Laboratory
University of California
Livermore, CA 94550

Saturation mechanisms of the lower-hybrid drift instability in the low drift velocity regime ($v_d \ll v_{\text{thermal ion}}$) are studied both in a 1d particle-hybrid simulation and a nonlinear perturbation theory; v_d is the relative drift velocity between the electrons and ions. We find that ion traping stabilizes the instability when v_d is kept constant, unless current relaxation ($v_d \to 0$) occurs via quasilinear diffusion. We also find a new saturation mechanism: a nonlinear ion orbit perturbation induces a frequency shift which is particularly effective in saturating long wavelength modes.

We use a one-dimensional slab configuration. In zero order, the ion pressure gradient cancels the equilibrium electric field force. in first order, the ions are treated as unmagnetized, and the electrons are assumed to respond to the wave linearly, because $\omega_{ci} \ll |\omega| \ll \omega_{pe}, \omega_{ce}$.

In simulation of small amplitude modes, there was good agreement of the linear growth rate, real frequency, and influence of finite beta effects associated with the nonresonant gradient B electron orbit modifications with linear theory. For large amplitude modes, at zero plasma beta and zero electron temperature, the simulations show that, when v_d is kept constant, the lower-hybrid drift instability is stabilized by ion trapping. When v_d is allowed to vary in time (for example, as a self-consistent consequence of momentum conservation), stabilization occurs as result of current relaxation with $v_d \to 0$, at a much lower level, a little below Davidson's prediction for $v_E/v_{ti} \lesssim 1$, as given by[1]

$$\frac{\mathcal{E}_s}{nT_i} = \frac{1}{8(1+\omega_{pe}^2/\omega_{ce}^2)} \frac{m_e}{m_i} \left(\frac{v_E}{v_{ti}}\right)^2 .$$

Analytic theory shows that a finite perturbation of the ion orbits leads to a nonlinear frequency shift that can stabilize the lower-hybrid drift instability. However, the resulting saturation level is small only for modes with wavelengths much longer than that of the most unstable mode. This result is obtained from a self-consistent solution of the Vlasov-Poisson equations using perturbation theory in which the nonlinear dielectric function and the nonlinear temporal evolution of a single unstable mode in the low drift velocity regime are calculated analytically.

*This research was supported in part by the Office of Naval Research under Contract N00014-77-c-0578, and in part by the Department of Energy under Contract No. W-7405-ENG-48.

[1]R. C. Davidson, Phys. Fluids 21, 1375 (1978).

INSTABILITIES DUE TO CURRENTS IN DIODE REGIONS

(C. K. Birdsall)

Interest in these instabilities has varied in time; some claim that this interest revives on about a seven year cycle, beginning with the work on limiting current (or perveance) by B. Salzberg and A. V. Haeff in the late 1930's and that of J. R. Pierce in the early 1940's. We may be near another peak now. While later cycles have tended to progress beyond earlier work, there is evidence that later workers have tended to miss earlier work.

Starting in 1959, our plasma theory and simulation group contributed some insights into these problems. One insight from simulation was that the diode current instabilities could grow into large amplitude oscillatory steady states ($\omega \approx \omega_p$). Another was that the time-average of the oscillatory current was larger than that obtained from time independent analysis.

A list follows of representative (but not exhaustive) papers of our group and related work done elsewhere in the 1960's. The papers themselves provide more references. We commend them to those beginning to work on current instabilities: in diode regions as such, or in sheaths, divertors, guns, accelerators, propulsion devices, direct converters, etc., etc.

Instabilities due to Currents in Diode Regions: Selected References in 1960's

1960

Lomax, R. J., Transient space-charge flow, J. Elec. and Cont. 9, pp. 127-140, August.

1961

Birdsall, C. K. and Bridges, W. B., Space-charge instabilities in electron diodes and plasma converters, J. Appl. Phys. 34, pp. 2611-2618, December.

Lomax, R. J., Unstable electron flow in a diode, Proc. I.E.E. Part C, 108, pp. 119-121, March.

1962

Bridges, W. B. and Birdsall, C. K., An electron stream instability, 185 pages, Tech. Rept. No. 60-443, E.R.L., Univ. of Calif., Berkeley, CA, March. (Bridges' Thesis)

1963

Bridges, W. B. and Birdsall, C. K., Space-charge instabilities in electron diodes, II, J. Appl. Phys. 34, pp. 2946-2955, October.

Buneman, O. and Kooyers, G. P., Computer simulation of the electron mixing mechanism in ion propulsion, A.I.A.A.J., 1, pp. 2525-2528.

1964

Burger, P., Nonexistence of dc states in low-pressure thermionic converters, J. Appl. Phys. 35, pp. 3048-3049, October.

Cutler, W. H., High frequency oscillations in a thermal plasma, J. Appl. Phys. 35, pp. 464-465, February.

1965

Bridges, W. B., Frey, J. I. and Birdsall, C. K., Limiting stable currents in bounded electron and ion streams, IEEE Trans. Electron Devices 12, pp. 264-272, May.

Burger, P., Theory of large amplitude oscillations in the one-dimensional low pressure cesium thermionic converter, J. Appl. Phys. 36, pp. 1938-1943, June.

Burger, P., Dunn, D. A. and Halsted, A. S., Computer experiments on the randomization of electrons in a collisionless plasma, Phys. Fluids 8, pp. 2263-2272, December.

Frey, J. I. and Birdsall, C. K., Electron stream diode instabilities with elastic collisions, J. Appl. Phys. 36, pp. 2962-2964, September. (See correction by Faulkner and Ware, 1969.)

Wadhwa, R. P., Buneman, O. and Brauch, D. F., Two-dimensional computer experiments on ion-beam neutralization, A.I.A.A.J. 3, 1076-1081, June.

1966

Birdsall, C. K. and Bridges, W. B., Electron Dynamics of Diode Regions, Academic Press, N. Y. (See Chap. 3, Stability of flow; nonlinear solution of multiparticle model.).

Brauch, D. F., Buneman, O. and Wadhwa, R. P., Computer studies of plasma boundaries and lens effects created by immersed and withdrawn neutralizers, A.I.A.A.J. 4, 651-653, April.

Cutler, W. H. and Burger, P., Oscillations in the thermal cesium plasma diode, J. Appl. Phys. 37, pp. 2867-2873, June.

Frey, J. I. and Birdsall, C. K., Instabilities in a neutralized electron stream in a finite length drift tube, J. Appl. Phys. 36, pp. 2962-2964, April (See correction by Faulkner and Ware, 1969.).

Twombly, J. C., Dynamic behavior of a long thin electron beam, IEEE Trans. on Elec. Dev., ED-13, pp. 934-942, December.

1967

Burger, P., Elastic collisions in simulating one-dimensional plasma diodes on the computer, Phys. Fluids 10, pp. 658-666, March.

Hirsch, R. L., Inertial-electrostatic confinement of ionized fusion gases, J. Appl. Phys. 38, pp. 4522-4534, October.

1968

Hockney, R. W., Formation and stability of virtual electrodes in a cylinder, J. Appl. Phys 39, pp. 4166-4170, August.

1969

Faulkner, J. E. and Ware, A. A., The effect of finite ion mass on the stability of a space-charge-neutralized electron beam, J. Appl. Phys. 40, pp. 366-368, January.

1970

Barnes, C. W., The computer simulation of a spherically symmetric plasma, SUIPR Report No. 344, Institute for Plasma Research, Stanford University, Stanford, CA, March.

1971

Dunn, Donald A., Models of Particles and Moving Media, Academic Press, New York (See Chap. 6, Motion of many interacting particles - the Lagrangian model.).

DISTRIBUTION LIST - 1

Department of Energy

Manley, Nelson, Price, Priester, Sadowsky, Siambis

Department of Navy

Condell, Roberson, Florance

Austin Research Associates

Drummond, Moore

Bell Telephone Laboratories

Hasegawa

Calif. State Ploytech. Univ.

Rathman

Columbia University

Chu

Cornell University

Mankofsky

Electrical Power Research Inst.

Gough, Scott

General Atomic Company

Helton, Lee

Georgia Institute of Technology

Bateman

Hascom Air Force Base

Rubin

IBM Corporation

Gazdag

JAYCOR

Klein, Tumolillo

Dory, Meier, Mook

Princeton Plasma Physics Lab.

Chen, Cheng, Lee, Okuda, Tang

Princeton University

Graydon

Science Applications, Inc.

McBride, Wagner

Sandia Laboratories

Freeman, Poukey, Quintenz

Stevens Institute

Rosen

Sonoma State University

Johnston

Stanford University

Buneman

University of Arizona

Morse

Univ. of California, Berkeley

Arons, Au-Yeung, Birdsall, Buchanan, Chen, Chorin, Friedman, Grisham, Harned, Hudson, Keith, Kim, Lichtenberg, Lieberman, McKee, Otani, Potter, Thomas

University of California, Davis

DeGroot, Woo

University of California, Irvine

Rynn

Univ. of Calif., Los Angeles

Dawson, Decyk, Huff, Lieuer, Lin, Tajima

DISTRIBUTION LIST - 2

Air Force Base

Genoni, Pettus

Los Alamos Scientific Laboratory

Barnes, Burnett, Forslund, Gitomer, Hewett, Lewis, Lindemuth, Lindman, Mason, Neilson, Oliphant, Sgro

Lawrence Berkeley Laboratory

Cooper, Feder, Kaufman, Kunkel, Pyle

Lawrence Livermore Laboratory

Albritton, Anderson, Brengle, Briggs, Bruijnes, Byers, Chambers, Cohen, Condit, Estabrook, Fawley, Finan, Fries, Fuss, Harte, Killeen, Kruer, Langdon, Lasinski, Lee, Maron, Marx, Matsuda, Max, McNamara, Mirin, Nevins, Nielson, Smith, Tull

Mass. Institute of Technology

Berman, Bers, Gerver, Kulp, Palevsky, Tetreault

Mission Research Corporation

Hobbs, Godfrey

NASA - Langley Research Center

Hohl

U.S. Naval Research Laboratory

Boris, Drobot, Haber, Orens, Vomvoridis, Winsor

Northwestern University

Crystal, Denavit

New York University

Grad, Weitzner

Oak Ridge National Laboratory

University of Iowa

Joyce, Knorr, Nicholson

University of Maryland

Guillory, Rowland, Sternlieb, Winske

University of Texas

Horton, MacMahon

University of Wisconsin

Shohet

Culham Laboratory

Eastwood, Roberts

University of Reading

Hockney

Ecole Polytechnique / Centre de Polytech.

Adam

Bhabha Atomic Research Centre

Aiyer

Gell

Tel-Aviv University

Cuperman

Nagoya University

Kamimura

Max Planck Inst. fur Plasmaphysik

Biskamp